

General Disclaimer

One or more of the Following Statements may affect this Document

- This document has been reproduced from the best copy furnished by the organizational source. It is being released in the interest of making available as much information as possible.
- This document may contain data, which exceeds the sheet parameters. It was furnished in this condition by the organizational source and is the best copy available.
- This document may contain tone-on-tone or color graphs, charts and/or pictures, which have been reproduced in black and white.
- This document is paginated as submitted by the original source.
- Portions of this document are not fully legible due to the historical nature of some of the material. However, it is the best reproduction available from the original submission.

DRA

OLD DOMINION UNIVERSITY RESEARCH FOUNDATION

DEPARTMENT OF MECHANICAL ENGINEERING AND MECHANICS
SCHOOL OF ENGINEERING
OLD DOMINION UNIVERSITY
NORFOLK, VIRGINIA

APPLICATION OF THE METHOD OF LINES FOR SOLUTIONS
OF THE NAVIER-STOKES EQUATIONS USING A NONUNIFORM
GRID DISTRIBUTION

By
Jamshid S. Abolhassani
and
S. N. Tiwari, Principal Investigator



Progress Report
For the period ending June 30, 1983

Prepared for the
National Aeronautics and Space Administration
Langley Research Center
Hampton, Virginia 23665

Under
Research Grant NCCI-68
Robert E. Smith, Jr., Technical Monitor

(NASA-CR-173180) APPLICATION OF THE METHOD
OF LINES FOR SOLUTIONS OF THE NAVIER-STOKES
EQUATIONS USING A NONUNIFORM GRID
DISTRIBUTION Progress Report, period ending
30 Jun. 1983 (Old Dominion Univ., Norfolk.

N84-16870
Unclas
G3/64 15044



August 1983



DEPARTMENT OF MECHANICAL ENGINEERING AND MECHANICS
SCHOOL OF ENGINEERING
OLD DOMINION UNIVERSITY
NORFOLK, VIRGINIA

APPLICATION OF THE METHOD OF LINES FOR SOLUTIONS
OF THE NAVIER-STOKES EQUATIONS USING A NONUNIFORM
GRID DISTRIBUTION

By

Jamshid S. Abolhassani

and

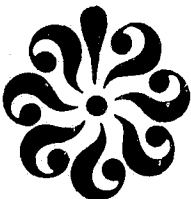
S. N. Tiwari, Principal Investigator

Progress Report
For the period ending June 30, 1983

Prepared for the
National Aeronautics and Space Administration
Langley Research Center
Hampton, Virginia 23665

Under
Research Grant NCCI-68
Robert E. Smith, Jr., Technical Monitor

Submitted by the
Old Dominion University Research Foundation
P.O. Box 6369
Norfolk, Virginia 23508



August 1983

FORWARD

This is a progress report on the work completed on the research project "Numerical Solution of Axisymmetric Flow with Arbitrary Wall Geometry." The period of performance on this research was June 1, 1982 through June 30, 1983. The work was supported by the NASA/Langley Research Center through the Cooperative Agreement NCCI-68. The cooperative agreement was monitored by Dr. Robert E. Smith, Jr., of the Analysis and Computational Division (Computer Science and Applications Branch), MS/125.

TABLE OF CONTENTS

	<u>Page</u>
FORWARD.....	ii
LIST OF FIGURES.....	v
LIST OF SYMBOLS.....	viii
SUMMARY.....	x
1. INTRODUCTION.....	1
2. THEORETICAL FORMULATION.....	5
2.1 Governing Equations.....	5
2.2 Stream Function-Vorticity Formulation.....	6
2.3 Coordinate Transformation.....	8
3. COMPUTATIONAL PROCEDURES.....	15
3.1 Stream Function Equation.....	15
3.2 Application of Successive Over Relaxation.....	17
3.3 The Application of the Method of Lines to the Vorticity Equation.....	20
3.3.1 Advantages and Disadvantages of the Method of Lines.....	21
3.3.2 Convergence, Accuracy, and Stability.....	21
4. STIFFNESS ANALYSIS	23
4.1 Effect of Grid Concentration on Stiffness.....	24
4.2 Effect of Differencing Schemes on Stiffness.....	27
5. BOUNDARY AND INITIAL CONDITIONS.....	36
5.1 Inlet Condition.....	37
5.2 Outlet Condition.....	39
5.3 Wall Condition.....	41
5.4 Symmetry Condition.....	42
5.5 Moving Wall Condition.....	42
5.6 Initial Condition.....	44
6. GRID GENERATION TECHNIQUES.....	45
6.1 Algebraic Method.....	46
6.2 Differential Method.....	48
7. PHYSICAL APPLICATIONS.....	50
7.1 Internal Flows.....	51
7.2 Driven Cavity.....	53

TABLE OF CONTENTS - CONCLUDED

	<u>Page</u>
8. RESULTS AND DISCUSSION.....	56
9. CONCLUSIONS.....	92
REFERENCES.....	95

LIST OF FIGURES

<u>Figure</u>	<u>Page</u>
2.1 Coordinate systems.....	9
3.1 Node numbering scheme.....	18
4.1 Stiffness characteristic for heat equation.....	28
4.2 Stiffness characteristic for fluid flow equation.....	31
4.3 Stability region for Adams-Bashforth (first order).....	32
4.4 Variation of step size with Reynolds number and number of grids point.....	34
5.1 Boundary conditions for various geometries.....	38
7.1 Physical model for duct flows.....	52
7.2 Curved-wall diffuser geometry.....	54
8.1 Grid distribution for parallel plates and pipe.....	57
8.2a Velocity distribution for flow between parallel plates, $Re = 200$	58
8.2b Stream function contours for flow between parallel plates, $Re = 200$	59
8.2c Vorticity contours for flow between parallel plates, $Re = 200$	60
8.3a Velocity distribution for pipe flow, $Re = 200$	61
8.3b Stream function contours for pipe flow, $Re = 200$	62
8.3c Vorticity contours for pipe flow, $Re = 200$	63
8.4a Velocity distribution for flow between parallel plates, $Re = 1000$	64
8.4b Stream function contours for flow between parallel plates, $Re = 1000$	65
8.4c Vorticity contours for flow between parallel plates, $Re = 1000$	66
8.5a Velocity distribution for pipe flow, $Re = 1000$	67
8.5b Stream function contours for pipe flow, $Re = 1000$	68

LIST OF FIGURES - CONTINUED

<u>Figure</u>		<u>Page</u>
8.5c	Vorticity contours for pipe flow, $Re = 1000$	69
8.6	Grid distribution for a diffuser, $\bar{\alpha} = 1$, $\theta = 5$, $L = 20$, $L_t = 32$	71
8.7a	Velocity distribution for a bell-type diffuser, $\bar{\alpha} = 1$, $\theta = 5$, $L = 20$, $L_t = 32$, $Re = 200$	72
8.7b	Vorticity contours for a bell-type diffuser, $\bar{\alpha} = 1$, $\theta = 5$, $L=20$, $L_t = 32$, $Re = 200$	73
8.7c	Stream function contours for a bell-type diffuser, $\bar{\alpha} = 1$, $\theta = 5$, $L = 20$, $L_t = 32$, $Re = 200$	74
8.8	Grid distribution for a bell-type diffuser, $\bar{\alpha} = 1$, $\theta = 10$, $L = 20$, $L_t = 40$	75
8.9a	Velocity distribution for a bell-type diffuser, $\bar{\alpha} = 1$, $\theta = 10$, $L = 20$, $L_t = 40$, $Re = 200$	76
8.9b	Stream function contours for a bell-type diffuser, $\bar{\alpha} = 1$, $\theta = 10$, $L = 20$, $L_t = 40$, $Re = 200$	77
8.9c	Vorticity contours for a bell-type diffuser, $\bar{\alpha} = 1$, $\theta = 10$, $L = 20$, $L_t = 40$, $Re = 200$	78
8.10	Uniform grid distribution for a driven cavity.....	79
8.11a	Stream function distribution for uniform grid distribution, $Re = 100$	80
8.11b	Vorticity distribution for uniform grid distribution, $Re = 100$	81
8.12a	Stream function distribution for uniform grid distribution, $Re = 1000$	82
8.12b	Vorticity distribution for uniform grid dis- tribution, $Re = 1000$	83
8.13a	Stream function distribution for uniform grid distribution, $Re = 10,000$	84

LIST OF FIGURES - CONCLUDED

<u>Figure</u>		<u>Page</u>
8.13b	Vorticity distribution for uniform grid distribution, $Re = 10,000$	85
8.14	Nonuniform grid distribution for a driven cavity.....	87
8.15a	Stream function distribution for nonuniform grids, $Re = 100$	88
8.15b	Vorticity distribution for nonuniform grids, $Re = 100$..	89
8.16a	Stream function distribution for nonuniform grids, $Re = 1,000$	90
8.16b	Vorticity distribution for nonuniform grids, $Re = 1,000$	91

LIST OF SYMBOLS

a, b, c	element of Matrix (A), Eq. (4.13)
a_i, b_i, c_i	coefficient of Eqs. (4.1) and (5.5)
AI, AO	inflow and outflow parameter, Eqs. (5.1) and (5.5)
A1, B1	coefficient of Eq. (2.21)
A2, B2	coefficient of Eq. (2.22)
f_1, f_2, f_3, f_4	blending function, Eqs. (6.11) and (6.12)
H(X)	step function, Eq. (7.1)
IM	imaginary part of the eigenvalue
$ J $	Jacobian of transformation
k	iteration number
K	concentration factor, Eq. (2.3)
L	characteristic length
L_t	total length of diffuser
NI, NO	inflow and outflow parameter
P	normalized pressure
r	radial coordinate (physical)
r_2	diffuser outlet radius
Re	Reynolds number
RE	real part of the eigenvalue
T	temperature
t	non-dimensional time
U_i, V_i	non-dimensional velocity components
U_∞	free stream velocity

LIST OF SYMBOLS - CONCLUDED

U_{\max}	maximum outlet velocity
z	axial coordinate (physical)
$\bar{\alpha}$	wall contouring parameter
α	μ/Re
η	radial (vertical) coordinate (computational)
δ	index, zero for two dimensional, one for axisymmetric flow
θ	angle of diffuser
ρ	density
μ	non-dimensional viscosity
μ_{∞}	free stream viscosity
ψ	stream function
ω	vorticity
ω_0	relaxation factor
ξ	axial coordinate (computational)
λ	eigenvalue

Subscripts

i, j, N	node number
-----------	-------------

APPLICATION OF THE METHOD OF LINES FOR SOLUTIONS OF
THE NAVIER-STOKES EQUATIONS USING A NONUNIFORM GRID DISTRIBUTION

By

J. S. Abolhassani¹ and S. N. Tiwari²

SUMMARY

The feasibility of the method of lines is investigated for solutions of physical problems requiring nonuniform grid distributions. To attain this, it was also necessary to investigate the stiffness characteristics of the pertinent equations. For specific applications, the governing equations considered are those for viscous, incompressible, two-dimensional and axisymmetric flows. These equations are transformed from the physical domain having a variable mesh to a computational domain with a uniform mesh. The two governing partial differential equations are the vorticity and stream function equations. The method of lines is used to solve the vorticity equation and the successive over relaxation technique is used to solve the stream function equation.

The method is applied to three laminar flow problems. These are: the flow in ducts, curved-wall diffusers, and a driven cavity. Results obtained for different flow conditions are in good agreement with available analytical and numerical solutions. The viability and validity of the method of lines are demonstrated by its application to Navier-Stokes equations in the physical domain having a variable mesh.

¹ Graduate Research Assistant, Department of Mechanical Engineering and, Mechanics, Old Dominion University, Norfolk, Virginia 23508.

² Eminent Professor, Department of Mechanical Engineering and Mechanics Old Dominion University, Norfolk, Virginia 23508.

Chapter 1

INTRODUCTION

In engineering and sciences, most physical phenomena may be described by a set of differential equations and boundary condition equations. These equations are mostly nonlinear in nature, and in a majority of cases, they can be solved only by numerical approaches. In particular, the field of fluid dynamics is governed by a specific set of nonlinear partial differential equations called the Navier-Stokes equations. In certain cases, flow fields may be described accurately by the incompressible form of the Navier-Stokes equations. For the present study, the incompressible form of the Navier-Stokes equations is expressed in terms of the stream function and vorticity. The resulting equations are two coupled nonlinear partial differential equations. The boundary conditions for the dependent variables, stream function and vorticity, are expressed by a set of coupled linear equations which depend on the nature of physical applications.

In the field of computational fluid dynamics, finite difference and finite element methods have a well developed history. Another method called "The Method of Lines (MOL)" has also received special attention for the numerical solution of certain partial differential equations. Detailed discussions on the method of lines are available in [1-8]*. If the governing equations contain both time and space variables, the procedure is to discretize the space variable components and treat the time varying component as a continuum. This leads to a system of coupled ordinary differential equations (ODE'S) which can be

*The number in brackets indicate references.

integrated with sophisticated ordinary differential equation software [9] having automated time-step control. The advantages of this approach are that the techniques can be applied quickly and the magnitude of knowledge about ordinary differential equation solvers can be utilized for obtaining specific solutions.

The early development of the method of lines was in the Soviet Union. Liskovet's article [1] is a review of 154 papers which date up to the mid-sixties. This review has considered linear partial differential equations of elliptic, parabolic, and hyperbolic types. Leser and Harrison [2], and Hicks and Wei [3] showed extensively the viability and validity of the method for linear partial differential equations. Later, Klunker et al. [4] used the method of lines to calculate nonlinear conical flows. It was concluded that the method of lines is a useful and versatile procedure for structuring the numerical solutions to nonlinear equations. Jones et al. [5] presented an extensive discussion for application of the method of lines in elliptic systems. It was concluded that a large number of lines may cause nonconvergence. However, this conclusion was based on results obtained from linear systems. Loeb and Schiesser [10] presented an elegant way to analyze the stability of the method of lines. It was concluded that higher order finite difference approximations to the spatial derivatives would improve the accuracy, stability and computational cost. Madsen and Sincovec [6] applied the method of lines for solution of several nonlinear partial differential equations. These problems were the diffusion of electrolytes, flow through porous media, and global atmospheric transport with kinetics. It was concluded that the method of lines gives satisfactory and reliable results which could not be

obtained by using the finite difference schemes. Hamilton [7] obtained solutions of axisymmetric and two-dimensional inviscid flow over blunt bodies using the method of lines and observed very accurate solutions using just a few lines. Kurtz et al. [8] applied the method of lines to the viscous stream function - vorticity equations in a rectangular coordinate system. The particular problem discussed was the flow in a driven cavity. It was concluded that the method of lines is capable of producing solutions to the stream function - vorticity equation at very high Reynolds numbers where standard finite difference techniques fail [11].

The literature survey indicates that the method of lines has been applied by several investigators in numerical experimentations using only the uniform grid distribution. For many physical problems, however, it becomes essential to have irregular grid distributions. This may be due to the complexity of the physical boundary geometry, and/or local grid resolution. Therefore, there exists a strong need for investigating the feasibility of the method of lines for physical domains that are covered with variable grids which conform to the boundary contours and may be concentrated in specified regions.

The objective of this study is to establish the validity and viability of the method of lines where there is an arbitrary grid distribution. Also, this study investigates the effects of grid concentration, Reynolds number, boundary conditions, and differencing schemes on stiffness and stability by using a one-dimensional advection - diffusion fluid flow equation and heat equation.

For viscous incompressible flow, the equations of motion are derived in two-dimensional and axisymmetric coordinate systems in Chap. 2. These equations are transformed from the physical domain having a variable grid to a computational domain with a uniform grid. The resulting equations are solved numerically. The method of lines is used to solve the vorticity equation and successive overrelaxation is used to solve the stream function equation. The computation procedure is presented in Chap. 3. The stiffness analysis is presented in Chap. 4. A discussion on appropriate boundary and initial conditions is given in Chap. 5. Information on grid generation is presented in Chap. 6. In this study, the grids are generated by an algebraic method which transforms the irregular physical domain into a uniform computational domain. For physical applications, specific problems considered are: the flow between horizontal ducts, curved-wall diffusers, and flow in a driven cavity. The applications are described in Chap. 7. Results are obtained for different flow conditions and are compared with available analytical and numerical solutions in Chap. 8. The viability and validity of the method of lines are illustrated by its applications to the incompressible Navier-Stokes equations.

Chapter 2

THEORETICAL FORMULATION

The theory of fluid dynamics is based upon a set of governing equations called the Navier-Stokes equations. For multi-dimensional flow, the equations are second order nonlinear parabolic-elliptic partial differential equations. The first-order boundary-layer forms of the Navier-Stokes equations are parabolic in nature and offer some computational conveniences. These equations, however, are not applicable in many realistic flow conditions such as reverse and separated flows. Therefore, it becomes essential to make use of the full Navier-Stokes equations in many flow situations of practical interest. A brief discussion of the basic governing equations used in this study is presented in this chapter.

2.1 Governing Equations

For viscous incompressible flow the equations of motion can be written in tensor notation as

$$\text{Momentum:} \quad \rho \frac{D\bar{U}_i}{Dt} = \frac{\partial \bar{P}}{\partial \bar{x}_i} + \frac{\partial}{\partial \bar{x}_j} \left[\bar{\mu} \left[\frac{\partial \bar{U}_i}{\partial \bar{x}_j} + \frac{\partial \bar{U}_j}{\partial \bar{x}_i} \right] \right] \quad (2.1)$$

$$\text{Continuity:} \quad \frac{\partial \bar{U}_i}{\partial \bar{x}_i} = 0 \quad (2.2)$$

It should be noted that in Eq. (2.1), $\bar{\mu}$ is constant in the case of laminar flow. For the sake of generality, Eqs. (2.1) and (2.2) can be nondimensionalized by introducing the following variables:

$$U_i = \frac{\bar{U}_i}{U_\infty}, \quad X_i = \frac{\bar{X}_i}{L}, \quad P = \frac{\bar{P}}{\rho U_\infty^2},$$

$$\mu = \frac{\bar{\mu}}{\mu_\infty}, \quad \tau = \frac{\bar{\tau}}{L/U_\infty} \quad (2.3)$$

A substitution of these variables in Eqs. (2.1) and (2.2) results in

$$\frac{DU_i}{Dt} = -\frac{\partial P}{\partial X_i} + \frac{\partial}{\partial X_j} \left\{ \alpha \left[\frac{\partial U_i}{\partial X_j} + \frac{\partial U_j}{\partial X_i} \right] \right\} \quad (2.4)$$

$$\frac{\partial U_i}{\partial X_i} = 0 \quad (2.5)$$

where $\alpha = \mu/Re$ (2.6)

Equations (2.4) and (2.5) can be written in two-dimensional cartesian or cylindrical coordinates as

$$\frac{\partial U}{\partial t} + v \frac{\partial U}{\partial r} + U \frac{\partial U}{\partial z} = -\frac{\partial P}{\partial z} + 2 \frac{\partial}{\partial z} \left(\alpha \frac{\partial U}{\partial z} \right) +$$

$$\left(\frac{1}{r} \right)^\delta \frac{\partial}{\partial r} \left[\alpha r^\delta \left(\frac{\partial v}{\partial z} + \frac{\partial U}{\partial r} \right) \right] \quad (2.7)$$

$$\frac{\partial v}{\partial t} + v \frac{\partial v}{\partial r} + U \frac{\partial v}{\partial z} = -\frac{\partial P}{\partial r} + 2 \frac{\partial}{\partial r} \left(\alpha \frac{\partial v}{\partial r} \right) +$$

$$\frac{\partial}{\partial z} \left[\alpha \left(\frac{\partial v}{\partial z} + \frac{\partial U}{\partial r} \right) \right] + \frac{2\alpha\delta}{r} \left(\frac{\partial v}{\partial r} - \frac{v}{r} \right) \quad (2.8)$$

$$\left(\frac{1}{r} \right)^\delta \frac{\partial}{\partial r} \left(r^\delta v \right) + \frac{\partial U}{\partial z} = 0 \quad (2.9)$$

Equations (2.7) to (2.9) are applicable to plane two-dimensional flows if $\delta = 0$ and to axisymmetry flows if $\delta = 1$.

2.2 Stream Function and Vorticity Formulations

There are now three equations, Eqs. (2.7) - (2.9), and three unknowns U , V , and P . Introducing the definitions of the stream

function and vorticity it is possible to reduce the number of equations to two and this eliminates the pressure. The definitions of the stream function and vorticity are:

$$\omega = \frac{\partial V}{\partial Z} - \frac{\partial U}{\partial r} \quad (2.10)$$

$$U = \left(\frac{1}{r}\right)^\delta \frac{\partial \psi}{\partial r} \quad (2.11)$$

$$V = -\left(\frac{1}{r}\right)^\delta \frac{\partial \psi}{\partial Z} \quad (2.12)$$

where ω is the vorticity and ψ is the stream function.

A combination of Eqs. (2.7) through (2.12) results in

$$\begin{aligned} \frac{\partial \omega}{\partial t} = & \alpha \left[\frac{\partial^2 \omega}{\partial Z^2} + \frac{\partial^2 \omega}{\partial r^2} + \delta \left[\frac{\partial \omega}{\partial r} - \frac{\omega}{r} \right] / r \right] - \\ & \left[\left[u-2 \frac{\partial \alpha}{\partial Z} \right] \frac{\partial \omega}{\partial Z} + \left[v-2 \frac{\partial \alpha}{\partial r} \right] \frac{\partial \omega}{\partial r} \right] + \left[\delta \omega \left[v + \frac{\partial \alpha}{\partial r} \right] / r \right] \\ & + \left[\frac{\partial^2 \alpha}{\partial Z^2} - \frac{\partial^2 \alpha}{\partial r^2} \right] \left[\frac{\partial V}{\partial Z} + \frac{\partial U}{\partial r} \right] + 2 \frac{\partial^2 \alpha}{\partial r \partial Z} \left[\frac{\partial V}{\partial r} - \frac{\partial U}{\partial Z} \right] \end{aligned} \quad (2.13)$$

$$\frac{\partial^2 \psi}{\partial Z^2} + \frac{\partial^2 \psi}{\partial r^2} - \frac{\delta}{r} \frac{\partial \psi}{\partial r} + \frac{\delta}{r} \omega = 0 \quad (2.14)$$

Equation (2.13) is the non-conservative form of the vorticity equation.

The conservative form can be obtained by multiplying the continuity equation by ω and adding it to Eq. (2.13) as

$$\begin{aligned} \frac{\partial \omega}{\partial t} = & \alpha \left\{ \frac{\partial^2 \omega}{\partial Z^2} + \frac{\partial^2 \omega}{\partial r^2} + \delta \left[\frac{\partial \omega}{\partial r} - \frac{\omega}{r} \right] / r \right\} - \\ & \left\{ \frac{\partial (U\omega)}{\partial Z} + \frac{\partial (V\omega)}{\partial r} - 2 \left[\frac{\partial \alpha}{\partial Z} \cdot \frac{\partial \omega}{\partial Z} + \frac{\partial \alpha}{\partial r} \cdot \frac{\partial \omega}{\partial r} \right] \right\} \\ & + \left\{ \frac{\delta \omega}{r} \frac{\partial \alpha}{\partial r} + \left[\frac{\partial^2 \alpha}{\partial Z^2} - \frac{\partial^2 \alpha}{\partial r^2} \right] \left[\frac{\partial V}{\partial Z} + \frac{\partial U}{\partial r} \right] \right. \\ & \left. + 2 \frac{\partial^2 \alpha}{\partial r \partial Z} \left[\frac{\partial V}{\partial r} - \frac{\partial U}{\partial Z} \right] \right\} \end{aligned} \quad (2.15)$$

The preceding equations are nonlinear parabolic-elliptic partial differential equations which can be solved numerically along with appropriate boundary and initial conditions.

2.3 Coordinate Transformations

The governing Eqs. (2.13) through (2.15) are expressed in physical coordinates. For many problems, the boundaries may be quite irregular (Fig. 2.1a). This requires special consideration for the application of boundary conditions such as interpolation or some kind of approximations. Also a local grid resolution is required in most practical problems, which makes it extremely difficult to solve the governing equations in the physical coordinates. Therefore, it becomes advantageous to transform Eqs. (2.13) through (2.15) into new computational coordinates. The computational domain is an idealized rectangular coordinate system where a uniform grid is specified (Fig. 2.1b). In other words, this transformation maps the z, r domain of the physical coordinates (Fig. 2.1a) into the ξ, η domain of the new computational coordinates (Fig. 2.1b). This transformation, however, adds considerable complexity to the equations of motion. The following chain rules are used in the transformation process:

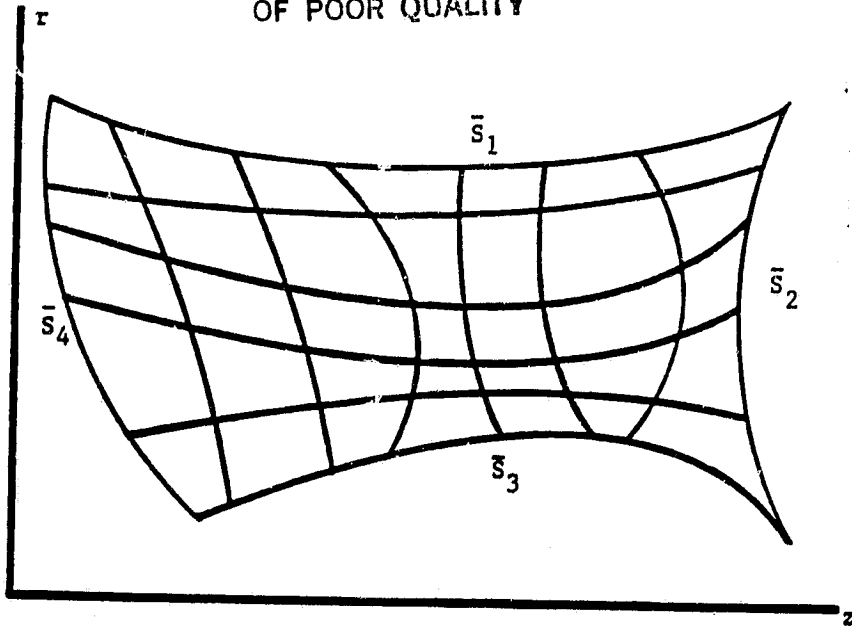
$$f_z = \xi_z f_\xi + \eta_z f_\eta \quad (2.16)$$

$$f_r = \xi_r f_\xi + \eta_r f_\eta \quad (2.17)$$

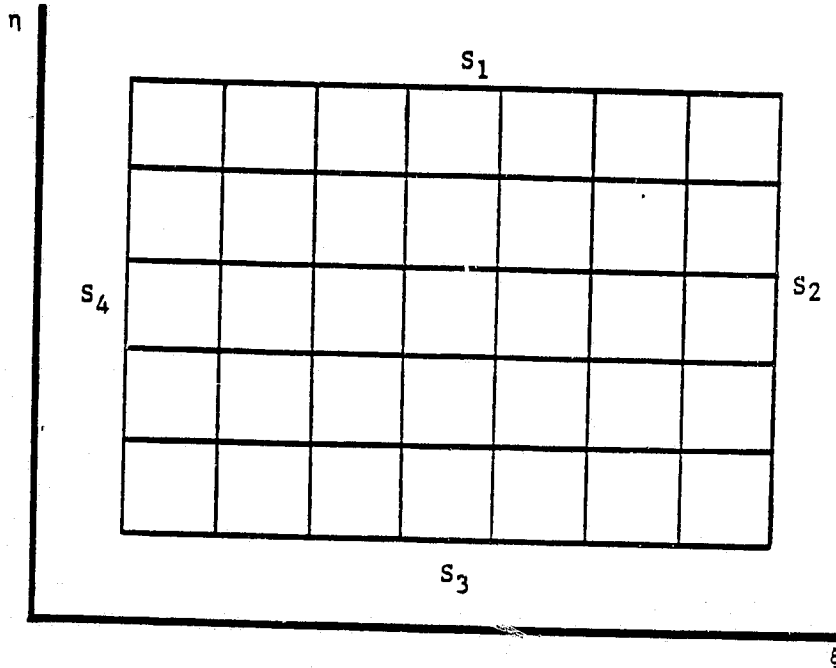
$$f_{rr} = \xi_r^2 f_{\xi\xi} + \xi_{rr} f_\xi + 2 \xi_r \eta_r f_{\xi\eta} + \eta_{rr} f_\eta + \eta_r^2 f_{\eta\eta} \quad (2.18)$$

$$f_{zz} = \xi_z^2 f_{\xi\xi} + \xi_{zz} f_\xi + 2 \xi_z \eta_z f_{\xi\eta} + \eta_{zz} f_\eta + \eta_z^2 f_{\eta\eta} \quad (2.19)$$

ORIGINAL PAGE 13
OF POOR QUALITY



(a) Physical coordinates.



(b) Computational coordinates.

Fig. 2.1 Coordinate systems.

$$f_{zr} = \xi_z \xi_r f_{\xi\xi} + \xi_{zr} f_{\xi} + (\xi_z \eta_r + \xi_r \eta_z) f_{\xi\eta} + \eta_{zr} f_{\eta} + \eta_z \eta_r f_{\eta\eta} \quad (2.20)$$

Equations (2.13) through (2.15) now can be written in terms of the transformed variables as

$$\omega_t = A_1 \omega_{\xi\xi} + B_1 \omega_{\xi} + C_1 \omega_{\xi\eta} + D_1 \omega_{\eta} + E_1 \omega_{\eta\eta} + F_1 \quad (2.21)$$

$$0 = A_2 \psi_{\xi\xi} + B_2 \psi_{\xi} + C_2 \psi_{\xi\eta} + D_2 \psi_{\eta} + E_2 \psi_{\eta\eta} + F_2 \quad (2.22)$$

For the non-conservative form of the vorticity equation, Eq. (2.21), the coefficients are defined as follows:

$$A_1 = \alpha (\xi_z^2 + \xi_r^2)$$

$$B_1 = \alpha [\xi_{zz} + \xi_{rr} + (\delta/r) \xi_r] - [U-2 (\xi_z \alpha_{\xi} + \eta_z \alpha_{\eta})] \xi_z - [V-2 (\xi_r \alpha_{\xi} + \eta_r \alpha_{\eta})] \xi_r$$

$$C_1 = 2\alpha (\xi_z \eta_z + \xi_r \eta_r)$$

$$D_1 = \alpha [\eta_{zz} + \eta_{rr} + (\delta/r) \eta_r] - [U-2 (\xi_z \alpha_{\xi} + \eta_z \alpha_{\eta})] \eta_z - [V-2 (\xi_r \alpha_{\xi} + \eta_r \alpha_{\eta})] \eta_r$$

$$E_1 = \alpha (\eta_z^2 + \eta_r^2)$$

$$\begin{aligned}
 F_1 = & (\delta\omega/r) [V + (\xi_r \alpha_\xi + \eta_r \alpha_\eta) - (\delta/r)] + [(\xi_z^2 - \xi_r^2) \alpha_{\xi\xi} \\
 & + (\xi_{zz} - \xi_{rr}) \alpha_\xi + 2(\xi_z \eta_z - \xi_r \eta_r) \alpha_{\xi\eta} + (\eta_{zz} - \eta_{rr}) \alpha_\eta \\
 & + (\eta_z^2 - \eta_r^2) \alpha_{\eta\eta}] [\xi_z v_\xi + \eta_z v_\eta + \xi_r u_\xi + \eta_r u_\eta] \\
 & + 2[\xi_z \xi_r \alpha_{\xi\xi} + \xi_{zr} \alpha_\xi + (\xi_z \eta_r + \xi_r \eta_z) \alpha_{\xi\eta} \\
 & + \eta_{zr} \alpha_\eta + \eta_z \eta_r \alpha_{\eta\eta}] [\xi_r v_\xi + \eta_r v_\eta - \xi_z u_\xi - \eta_z u_\eta]
 \end{aligned}$$

For laminar flow these coefficients will be reduced to the following:

$$A_1 = \alpha (\xi_z^2 + \xi_r^2)$$

$$B_1 = \alpha [\xi_{zz} + \xi_{rr} + (\delta/r) \xi_r] - U \xi_z - V \xi_r$$

$$Q_1 = 2\alpha (\xi_z \eta_z + \xi_r \eta_r)$$

$$D_1 = \alpha (\eta_{zz} + \eta_{rr} + \delta \eta_r / r) - U \eta_r - V \eta_z$$

$$E_1 = \alpha (\eta_z^2 + \eta_r^2)$$

$$F_1 = (\delta\omega/r) (V - \alpha/r)$$

For the conservative form of the vorticity equation, Eq. (2.15), the corresponding coefficients are

$$A_1 = \alpha (\xi_r^2 + \xi_z^2)$$

$$B_1 = \alpha [\xi_{zz} + \xi_{rr} + (\delta/r) \xi_r]$$

$$Q_1 = 2\alpha (\xi_z \eta_z + \xi_r \eta_r)$$

$$D_1 = \alpha \left[\eta_{zz} + \eta_{rr} + (\delta/r) \eta_r \right]$$

$$E_1 = \alpha \left(\eta_z^2 + \eta_r^2 \right)$$

$$F_1 = \left[\frac{\alpha \omega \delta}{r^2} + \xi_r \frac{\partial (V\omega)}{\partial \xi} + \eta_r \frac{\partial (V\omega)}{\partial \eta} + \xi_z \frac{\partial (U\omega)}{\partial \xi} + \eta_z \frac{\partial (U\omega)}{\partial \eta} \right]$$

The coefficients for the stream function equation, Eq. (2.22), are defined as follows:

$$A_2 = \xi_z^2 + \xi_r^2$$

$$B_2 = \xi_{zz} + \xi_{rr} - (\delta/r) \xi_r$$

$$C_2 = 2(\xi_z \eta_z + \xi_r \eta_r)$$

$$D_2 = \eta_{zz} + \eta_{rr} - (\delta/r) \eta_r$$

$$E_2 = \eta_z^2 + \eta_r^2$$

$$F_2 = r^\delta \omega$$

Equations (2.11) and (2.12) are written in the transformed coordinates as

$$U = (1/r)^\delta \left(\xi_r \psi_\xi + \eta_r \psi_\eta \right) \quad (2.23)$$

$$V = -(1/r)^\delta \left(\xi_z \psi_\xi + \eta_z \psi_\eta \right) \quad (2.24)$$

The next step is to establish relations between the physical and computational coordinates such that

$$\begin{aligned} z &= z(\xi, \eta) \\ r &= r(\xi, \eta) \end{aligned} \quad (2.25)$$

The above relations should be unique, single-valued and have continuous derivatives. This will be true if the determinant of the Jacobian matrix of Eq. (2.25) exists and is nonzero. The Jacobian matrix of the transformation is expressed as

$$J = \begin{bmatrix} z_{\xi} & z_{\eta} \\ r_{\xi} & r_{\eta} \end{bmatrix} \quad (2.26)$$

The inverse transformation of Eq. (2.25) and its Jacobian matrix can be written as

$$\begin{bmatrix} \xi \\ \eta \end{bmatrix} = \begin{bmatrix} \xi(z, r) \\ \eta(z, r) \end{bmatrix} \quad (2.27)$$

$$J^* = \begin{bmatrix} \xi_z & \xi_r \\ \eta_z & \eta_r \end{bmatrix} \quad (2.28)$$

Equations (2.26) and (2.28) are related by

$$J = [J^*]^{-1} \quad (2.29)$$

The relations between derivatives of the physical coordinates can be deduced from Eq. (2.29) as

$$\begin{aligned} \xi_z &= \frac{r_{\eta}}{|J|} & \eta_z &= -\frac{r_{\xi}}{|J|} \\ \xi_r &= -\frac{z_{\xi}}{|J|} & \eta_r &= \frac{z_{\eta}}{|J|} \end{aligned} \quad (2.30)$$

where $|J|$ is the Jacobian determinant.

The relations between the second derivatives can be obtained by using Eqs. (2.16), (2.17) and (2.30) as

$$\xi_{zz} = (\xi_z r_{\xi\eta} + \eta_z r_{\eta\eta} - \xi_z^2 J_{\xi} - \xi_z \eta_z J_{\eta}) / |J| \quad (2.31a)$$

$$\xi_{rr} = -(\eta_r z_{\eta\eta} + \xi_r z_{\xi\eta} + \xi_r \eta_r J_{\eta} + \xi_r^2 J_{\xi}) / |J| \quad (2.31b)$$

$$\xi_{rz} = -(\xi_z z_{\xi\eta} + \eta_z z_{\eta\eta} + \xi_r \xi_z J_{\xi} + \xi_r \eta_z J_{\eta}) / |J| \quad (2.31c)$$

$$\eta_{zz} = -(\xi_z r_{\xi\xi} + \eta_z r_{\xi\eta} + \xi_z \eta_z J_{\xi} + \eta_z^2 J_{\eta}) / |J| \quad (2.31d)$$

$$\eta_{rr} = (\eta_r z_{\xi\eta} + \xi_r z_{\xi\xi} - \xi_r \eta_r J_{\xi} - \eta_r^2 J_{\eta}) / |J| \quad (2.31e)$$

$$\eta_{rz} = -(\eta_r r_{\xi\eta} + \xi_r r_{\xi\xi} + \eta_z \eta_r J_{\eta} + \xi_r \eta_z J_{\xi}) / |J| \quad (2.31f)$$

Equations (2.30) and (2.31) relate derivatives of physical coordinates to computational coordinates; these derivatives should exist.

Chapter 3

COMPUTATIONAL PROCEDURES

The governing equations, Eqs. (2.13)-(2.15), are derived in Chap. 2 for incompressible flow in physical coordinates. These equations are transformed to new computational coordinates, as Eqs. (2.21) and (2.22). As mentioned before, these are full parabolic-elliptic partial differential equations, which are controlled by the boundary conditions for all variables along a surface which encloses the domain of interest. In case of turbulent flow, the equations are completed by supplying some auxiliary transport property relations. Because of the complexity of the equations there are only few analytical solutions. However, the equations can be solved using numerical techniques such as finite difference method or finite element method. There is also the method of lines (MOL). In the present study, the stream-function equation is solved by the successive overrelaxation (SOR) method and the vorticity equation is solved by the method of lines.

3.1 Stream Function Equation

The stream-function equation, Eq. (2.22), is a two-dimensional elliptic partial differential equations. Discretization of Eq. (2.22) yields a system of linear equations which should be solved at each iteration. There are several methods available to solve this equation some of which are listed below:

1. Direct methods

2. Richardson's method (point iteration)
3. Liebman's method (Gauss-Seidel)
4. Successive overrelaxation (extrapolated Liebman method)
5. Alternating directions implicit methods
6. Hopscotch methods

Since only the right hand side of this linear system, Eq. (2.22), changes at each iteration, it can be solved by the inversion method. This method sometimes is called the direct method. This is an efficient method for small systems, but the round off error destroys the accuracy of solution for large systems.

The Richardson's method is also known as the Gauss iteration or point iteration method. As mentioned before, discretization of Eq. (2.22) yields a system of linear equations which can also be solved iteratively. The computation is based on values computed in the previous iteration, i.e.,

$$\psi_N^{k+1} = F[\psi(N, k)] \quad (3.1)$$

where k is the iteration number. This iterative computation is carried out until some convergence criteria is satisfied.

Liebman's method is like Richardson's method except it uses all updated values at each iteration step, i.e.,

$$\psi_N^{k+1} = F[\psi(N, k, k+1)] \quad (3.2)$$

For better accuracy and efficiency, the results from Liebman's method may be extrapolated as

$$\psi_N^{k+1} = \psi_N^k + \omega_0 f[\psi(N, k, k+1)] \quad (3.3)$$

where $\omega_0 > 0$

In the preceding equation, ω_0 is a relaxation parameter. If the value of ω_0 is between one and two ($1 < \omega_0 < 2$), it represents overrelaxation, and if ω_0 is less than one ($0 < \omega_0 < 1$), it represents underrelaxation. Use of the over-relaxation method usually is not recommended for those equations which contain strong source terms. It has been found experimentally [12] that ω_0 is inversely proportional to Reynolds number. Therefore, underrelaxation is required as the Reynolds number is increased.

Extensive discussions on alternating directions implicit (ADI) and hopscotch methods are available in [11-13] and are not discussed any further here.

3.2 Successive Overrelaxation Formulation

In this study the successive overrelaxation (SOR) technique is formulated in such a way that a one-dimensional array is used to compute and store each variable. A typical node arrangement for SOR is shown in Fig. 3.1. By using second order differencing, Eq. (2.22) is expressed as

$$\begin{aligned} A_2 (\psi_{N+1}^k - 2\psi_N^{k+1} + \psi_{N-1}^{k+1}) + \frac{B_2}{2} [\psi_{N+1}^k - \psi_{N-1}^{k+1}] \\ + \frac{C_2}{4} [\psi_{N+IN+1}^k - \psi_{N+IN-1}^k + \psi_{N-IN-1}^{k+1} - \psi_{N-IN+1}^{k+1}] \\ + D_2 [\psi_{N+IN}^k - \psi_{N-IN}^{k+1}] + E_2 [\psi_{N+IN}^k - 2\psi_N^{k+1} + \psi_{N-IN}^{k+1}] + F_2 = 0 \end{aligned} \quad (3.4)$$

ORIGINAL PAGE IS
OF POOR QUALITY

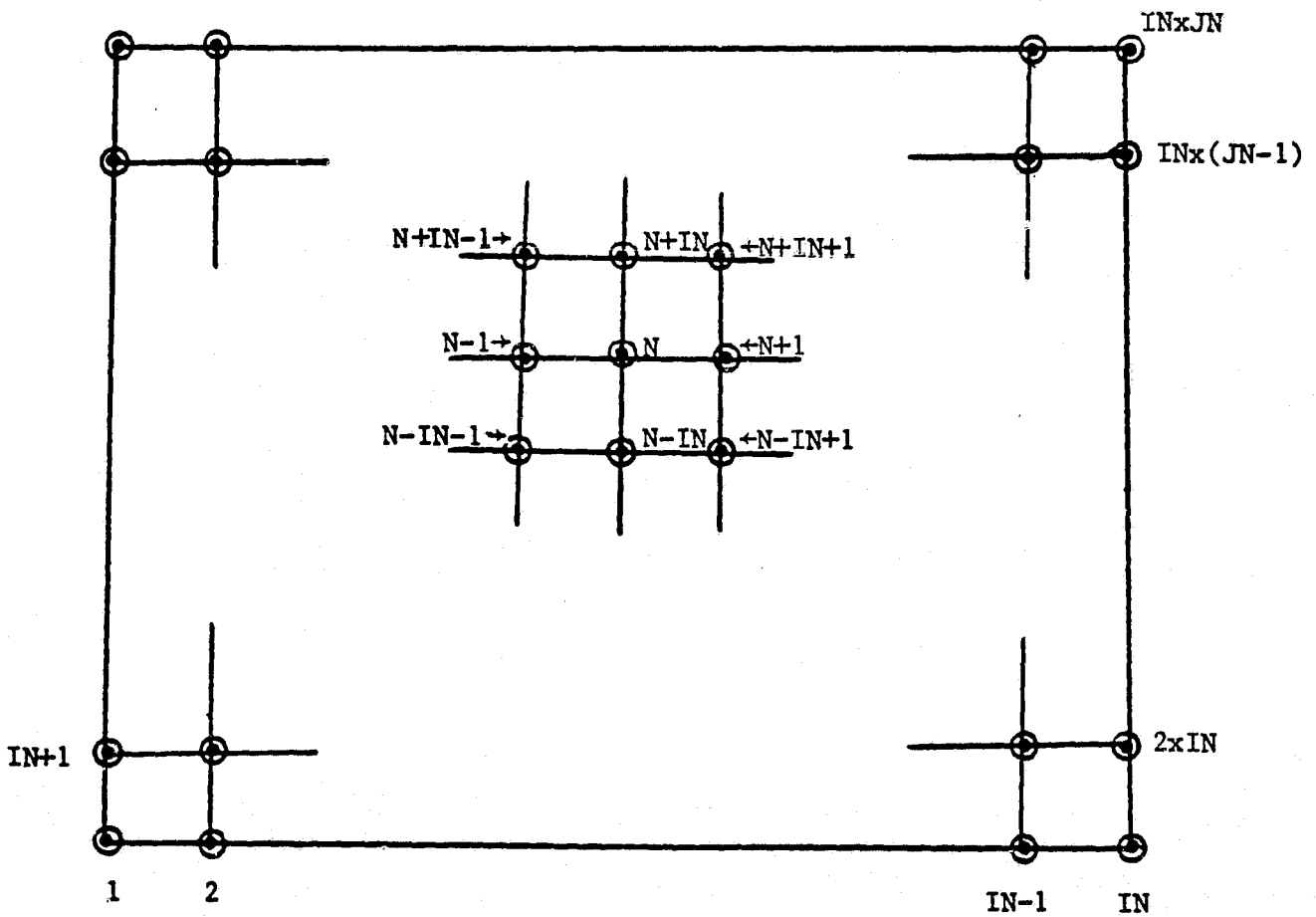


Fig. 3.1 Node numbering scheme.

Note that the coefficients are evaluated at the Nth node point.

Rearrangement of Eq. (3.4) results in

$$\psi_N^{k+1} = \psi_N^k + \frac{\text{Residual}(k, k+1, N)}{2(A_2 + E_2)} \quad (3.5)$$

where the Residual (k, k+1, N) is defined as

$$\begin{aligned} \text{Residual}(k, k+1, N) = & \frac{(2A_2 + B_2)}{2} \psi_{N+1}^k + \frac{2A_2 - B_2}{2} \psi_{N-1}^{k+1} \\ & + \frac{C_2}{4} [\psi_{N+IN+1}^k - \psi_{N+IN-1}^k + \psi_{N-IN-1}^{k+1} - \psi_{N-IN+1}^{k+1}] \\ & + \frac{2E_2 + D_2}{2} \psi_{N+IN}^k + \frac{2E_2 - D_2}{2} \psi_{N-IN}^k - 2(A_2 + E_2) \psi_N^{k+F_2} \end{aligned} \quad (3.6)$$

Equation (3.5) is Liebman's method, which can be improved by appropriate extrapolation

$$\psi_N^{k+1} = \psi_N^k + \frac{\omega_0}{2(A_2 + E_2)} \text{Residual}(k, k+1, N) \quad (3.7)$$

There is no analytical way to find the optimal relaxation factor (ω_0) for this case. However, one may use the optimal relaxation factor for the Poisson's equation with Dirichlet boundary conditions [12]. This is given by

$$\omega_0 = 2[1 - \sqrt{1-C} / C] \quad (3.8a)$$

where,
$$C = \left[\frac{\cos\left(\frac{\pi}{IN-1}\right) + \cos\left(\frac{\pi}{JN-1}\right)}{2} \right]^2 \quad (3.8b)$$

In Eq. (3.8b), IN and JN are the number of grid points in the axial and the vertical (radial) directions respectively.

3.3 Application of the Method of Lines to the Vorticity Equation

In the vorticity equation, the spatial derivatives are replaced by a corresponding set of second order difference equations. Also, the vorticity is considered to be continuous in time. This gives

$$\begin{aligned} \frac{d\omega}{dt} = & A_1 (\psi_{N+1} - 2\psi_N + \psi_{N-1}) + B_1 (\psi_{N+1} - \psi_{N-1})/2 \\ & + Q (\psi_{N+IN+1} - \psi_{N+IN-1} + \psi_{N-IN-1} - \psi_{N-IN+1})/4 \\ & + D_1 (\psi_{N+IN} - \psi_{N-IN})/2 + E_1 (\psi_{N+IN} - 2\psi_N + \psi_{N-IN}) + F_1 \end{aligned} \quad (3.9)$$

Equation (3.9) is a set of coupled ordinary differential equations, which should be integrated simultaneously.

The method of lines is used for solving the system of partial differential equations. As mentioned in the introduction, the method was developed and used originally in the Soviet Union. Liskovet's review article [1] is a review of 154 papers which date up to the mid-sixties. This review has considered linear partial differential equations of elliptic, parabolic, and hyperbolic types.

The method of lines basically changes a partial differential equation to a set of ordinary differential equation which can be integrated numerically. In the case of time dependent partial differential equations, the procedure is to discretize the spatial variable and treat the temporal variable as continuous in time. This

semi-discretization results in a set of ordinary differential equations, which can be integrated along the lines of time.

3.3.1 Advantages and Disadvantages of the Method of Lines

Finite difference and finite element techniques are well-developed and in general they are more attractive in terms of efficiency. Solutions of partial differential equations using these two methods lead to a system of linear algebraic equations which can be solved by direct or iterative methods. However, the nonlinear terms in the equations must be linearized. In the method of lines, there is no need for linearization. Other advantages are as follows: (1) possible establishment of convergence and stability criteria for a wide class of problems [3, 14], (2) accurate solutions by using higher order approximations for the derivatives and with less computational costs in comparison to the finite difference method, and (3) more efficient due to a better time-step control and easier implementation even for nonlinear systems.

There are certain limitations in the method of lines such as the number of lines. Jones and et al. [5] estimated that error is equal to $\exp [4N^4 / \pi b]$, where N is the number of lines and b is the characteristic length. This means that using a large number of lines (for better resolution) may bring significant instability. The former conclusion is valid for elliptic systems.

3.3.2 Convergence, Accuracy, and Stability

Convergence exists when the solution approaches the solution of original continuum differential equations as step size or grid size approaches zero. But, instability occurs when round off error or any other computational errors become unbounded. There are extensive

discussions about convergence and stability by Jones et al. [5], and Loeb and Schiesser [10]. Their results show that using higher order finite difference approximations for derivatives improves the accuracy and the stability, and reduces computer cost. They have also shown that using more grid points improves the accuracy, but makes the solution become less stable. Stability may be related to the stiffness of the equations. This effect is investigated in the next chapter.

Chapter 4
STIFFNESS ANALYSIS

In engineering problems, stiffness may arise due to the physics of the problem or be introduced to the problem because of the type of approach applied for obtaining solutions. An example is a problem involving chemical reactions where time scales span from 10^{-6} to 10^5 seconds, simultaneously. This system is referred to as a stiff system when the processes are coupled and when all time scales must be resolved. In mathematical terms, when the eigenvalues of a system of differential equations have a large variation, the system is referred to as a stiff system. For example, consider the following equation:

$$\dot{y} = Ay, \quad \text{where } A = \begin{bmatrix} -1 & 49 & 0 \\ 0 & -50 & 0 \\ 0 & 1150 & -1200 \end{bmatrix} \quad (4.1)$$

This equation has a solution of the form

$$\begin{aligned} Y_1(x) &= e^{-x} + e^{-50x} \\ Y_2(x) &= e^{-50x} \\ Y_3(x) &= e^{-50x} + e^{-1200x} \end{aligned}$$

The eigenvalues of this system vary from -1200 to -1. The degree of stiffness is measured by the stiffness ratio which is the ratio of the

largest eigenvalue to the smallest eigenvalue of the system. For example, the stiffness ratio for Eq. (4.1) is 1200. Stiffness may be a local problem in which case the equations are stiff in some regions and nonstiff in other regions. Numerical integration of Eq. (4.1) requires a specified integration step size h which is determined only by the components of the eigenvalues, λ_i and the stability region of the integration scheme. The stability of numerical integration of Eq. (4.1) is governed by the maximum absolute value of λ_i . For example, using Euler's method for the integration, it is necessary that $\{\text{Max}(\lambda_i)\} \cdot h < 2$ [15]. This implies that the maximum stable step size is $1/600$, meaning that 600 integration steps are required to reach $x = 1$.

There are only a limited number of numerical methods available to solve ordinary differential equations which utilize the stiffness characteristic [9, 14-17]. A popular method is the Gear's method [9, 14, 17]. Subroutine VOADAM [9] has been used to solve Eq. (3.9), which has the options for stiff and nonstiff systems. Stiff and nonstiff options differ in storage and computer time. The computer memory required for a stiff solver is of order N^2 (N number of equations), whereas for a nonstiff solver it is of order N . However, the stiff option generally requires much less computer time. As an example, Madsen and Sincovec [6] observed a 400% computer time saving by using a stiff integrator.

4.1 Effect of Grid Concentration on Stiffness

In many physical problems, one desires to have an arbitrary grid distribution with concentration at any location in the physical domain. In particular in flow field computation, concentrations are required

to capture rapid changes in flow conditions such as boundary layer, shock, and separation. Concentrations affect the stiffness characteristics of a system, and it is essential to investigate the effects of grid concentration on stiffness. For this purpose, a simple one-dimensional heat equation is considered. The equation is given by:

$$\frac{\partial T}{\partial t} = \frac{\partial^2 T}{\partial x^2}, \quad 0 < x < 1 \quad (4.2)$$

Equation (4.2) is transformed from the physical coordinate (x) into a computational coordinate (η)

$$\frac{\partial T}{\partial t} = \eta_x^2 T_{\eta\eta} + \eta_{xx} T_{\eta} \quad (4.3)$$

$$\text{where } \eta = \eta(x), \quad 0 < \eta < 1 \quad (4.4)$$

In Eq. (4.3), the spatial derivatives are discretized using a second-order finite-difference approximation and T is assumed to be continuous in time. This results in

$$\frac{dT_i}{dt} = a_i T_{i+1} + b_i T_i + c_i T_{i-1} \quad (4.5)$$

where

$$a_i = (\eta_x / \Delta\eta)^2 + \eta_{xx} / (2\Delta\eta) \quad (4.6a)$$

$$b_i = 2(\eta_x / \Delta\eta)^2 \quad (4.6b)$$

$$c_i = (\eta_{xx} / 2\Delta\eta) \quad (4.6c)$$

Equation (4.5) represents a set of ordinary differential equations which can be written in matrix form as

$$\frac{dT}{dt} = [A] T \quad (4.7)$$

where $[A] =$

$$\begin{bmatrix} b_1 & c_1 & & & \\ a_2 & b_2 & c_2 & & \\ & & a & b & c \\ & & & N-1 & \\ & & & a_N & b_N \end{bmatrix}$$

Eigenvalues of matrix $[A]$ are determined in order to analyze the stiffness characteristics. Eigenvalues of matrix $[A]$ depend on boundary conditions and the relation between physical and computational coordinates.

Consider the following relation between x and η , and the boundary conditions:

$$x = b(e^{K\eta} - 1) \quad (4.8a)$$

$$b = \left(\frac{K}{e - 1} \right)^{-1} \quad (4.8b)$$

$$T(0) = \frac{\partial T(1)}{\partial x} = 0 \quad (4.8c)$$

In the above equation, K is a stretching factor which determines the degree and location of the grid concentration. A large positive value of K results in a high grid concentration near $x = 0$, whereas a large negative value of K results in a high grid concentration near the $x = 1$ boundary. A substitution of Eq. (4.8) into Eq. (4.6) results in

$$a_i = \frac{e^{-2K\eta_i}}{(\Delta\eta Kb)^2} - \frac{e^{-2K\eta_i}}{2Kb^2\Delta\eta} \quad (4.9a)$$

$$b_i = \frac{-2e^{-2K\eta_i}}{(\Delta\eta Kb)^2} \quad (4.9b)$$

$$c_i = \frac{e^{-2K\eta_i}}{(\Delta\eta Kb)^2} + \frac{e^{-2K\eta_i}}{2Kb^2\Delta\eta} \quad (4.9c)$$

Eigenvalues of matrix $[A]$ are found numerically using subroutine REQR [18], and the stiffness ratios are computed for different values of stretching factors. Figure 4.1 shows a plot of the stretching factor versus the stiffness ratio. The plot indicates that stiffness increases with the magnitude of the stretching factor. Also, the slope of the stiffness characteristic curve is higher near the fixed boundary ($x=0$) than near the derivative boundary ($x=1$).

4.2 Effects of Differencing Scheme on Stiffness

In the finite difference approach, convergence and stability of a solution depend on the differencing scheme used. Similarly, the differencing scheme affects the stiffness of the resulting ordinary differential equation system in the method of lines. To investigate the effects of differencing schemes on stiffness, consider the linearized one-dimensional advection-diffusion fluid flow equation:

$$\frac{\partial \omega}{\partial t} = -U \frac{\partial \omega}{\partial x} + \frac{1}{Re} \frac{\partial^2 \omega}{\partial x^2} \quad (4.10)$$

ORIGINAL PAGE IS
OF POOR QUALITY

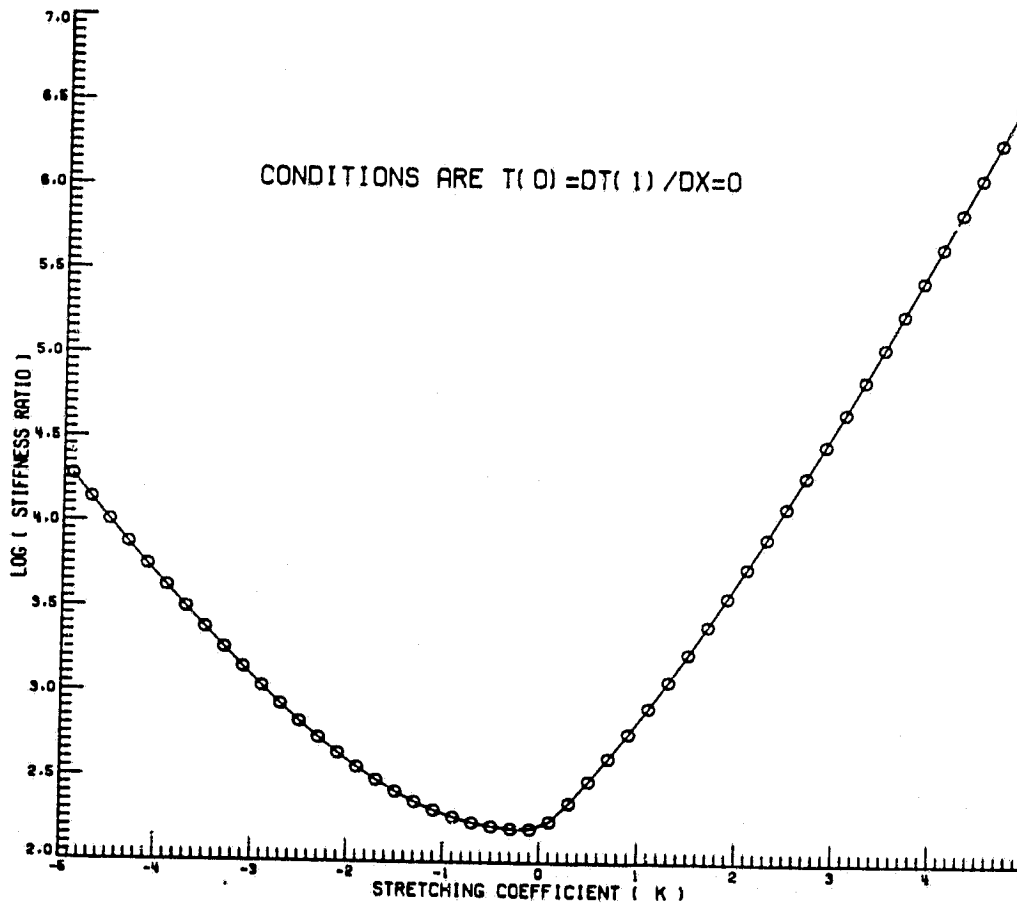


Fig. 4.1 Stiffness characteristic for heat equation.

For central differencing, they are

$$a = N^2 / Re + N/2, \quad b = -2N^2 / Re, \quad c = N^4 / Re - N/2$$

The eigenvalues of matrix [A] can be computed analytically, and they are

$$\lambda_n = b + 2 \sqrt{ac} \cos \frac{n\pi}{N+1} \quad (4.14)$$

A system of ordinary differential equations (e.g., Eq. 4.12) is unstable if the real parts of its eigenvalues are positive. Therefore, backward and central differencing are inherently stable, whereas forward differencing is conditionally stable, provided $Re < 2N$. It is shown later that forward differencing is not useful for solution of Eq. (4.10).

Stiffness ratios for these differencing schemes are computed and are plotted on Fig. 4.2. The plots show that the equations become stiff as the number of grid points is increased (curves 1-3), and the stiffness ratios do not depend on the differencing scheme at low Reynolds number (curves 4 and 5)

A specified integration step size is required for the integration of ordinary differential equations. Maximum allowable step size depends on the eigenvalues and the applied integration techniques. The step size should be selected such that λh is located in the stability region (Fig. 4.3). For instance, the stability region is shown in Fig. 4.3 for the Adams-Bashforth method (first order) where h is the step size and λ is the eigenvalue. Generally, the integration step size is inversely proportional to the distance between the location of the eigenvalue λ and the stability region. For example, if λ_A , λ_B , and

ORIGINAL PAGE IS
OF POOR QUALITY

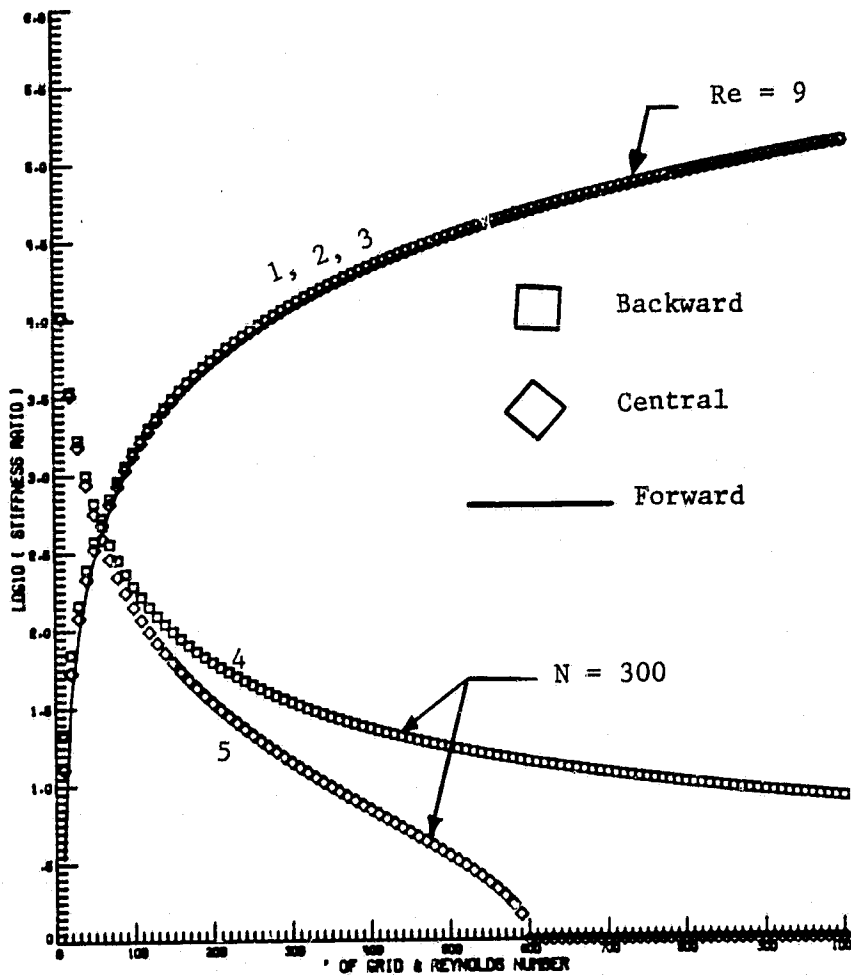


Fig. 4.2 Stiffness characteristic for fluid flow equation.

ORIGINAL PAGE IS
OF POOR QUALITY

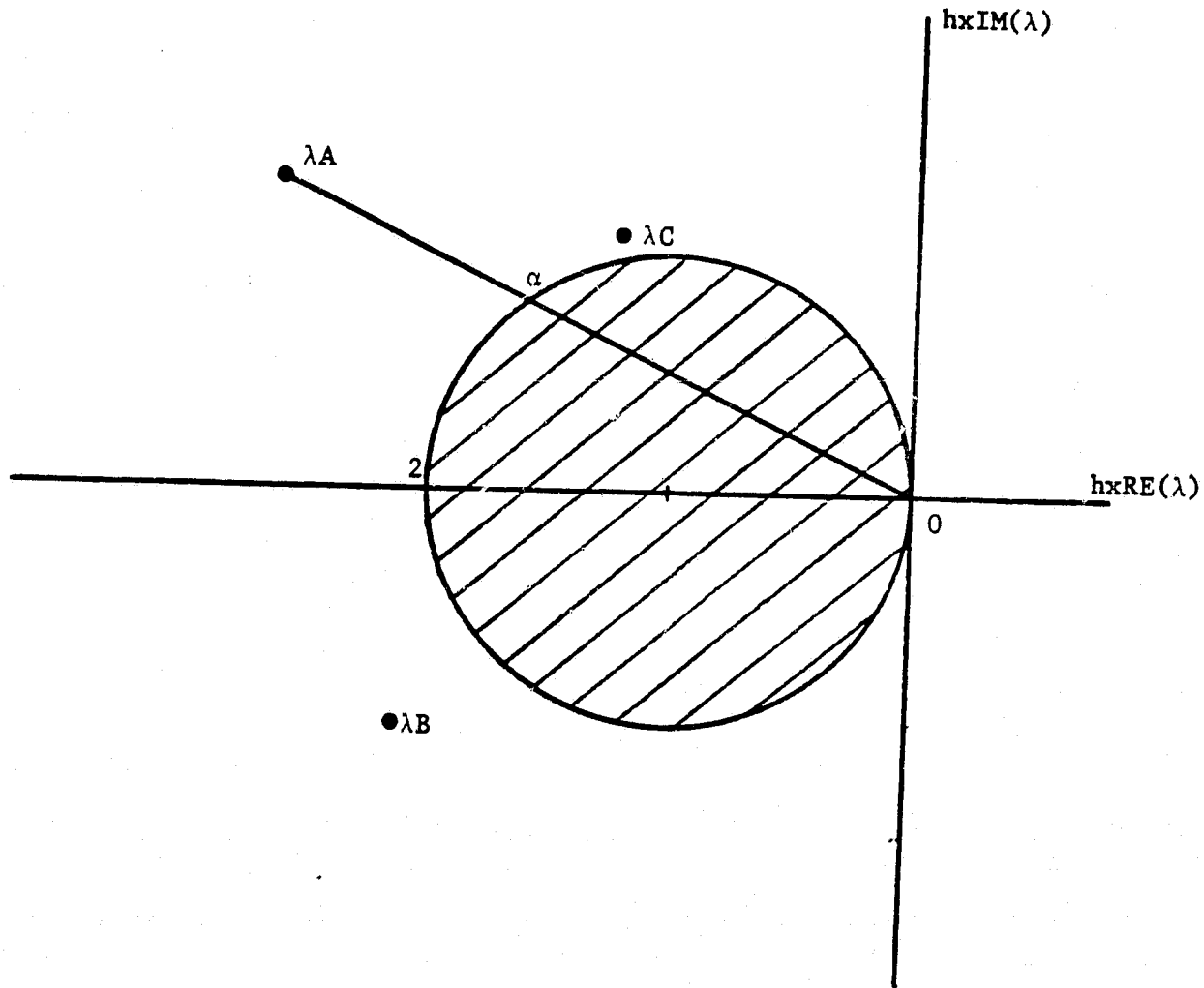


Fig. 4.3 Stability region for Adams-Bashforth (first order).

λ_C are the largest eigenvalues of three different systems of ordinary differential equations (Fig. 4.3), system A requires the smallest step size, because λ_A has the farthest distance from the stability region. The maximum allowable step size can be computed analytically for the Adams-Bashforth technique (first order). Consider eigenvalue λ_A [$\lambda_A = \text{RE}(\lambda) + i \text{IM}(\lambda)$], where RE is the real part and IM is the imaginary part, the step size should be selected such that the point A in the complex plane can be moved to the stability region. This requires

$$h_{\text{Max}} [\text{Modulus of } \lambda_A] = [\text{Modulus of } \lambda_a] \quad (4.15)$$

where from Fig. 4.3 Modulus of $\lambda_A = A0$, Modulus of $\lambda_a = a0$.

After some algebraic manipulation, the maximum step size is found to be

$$h_{\text{Max}} = \frac{-2\text{RE}}{[\text{Modulus of } \lambda_A]^2} \quad (4.16)$$

Using this equation, the step size can be computed for the different differencing schemes. In case of forward differencing, the step size is positive if $\text{Re} > 2N$, and the system is unstable. Therefore, it is impossible to solve Eq. (4.11) using forward differencing along with the Adams-Bashforth (first order) integration technique. Similarly, step size for central differencing is

$$h_{\text{Max}} \propto 1/\text{Re}. \quad (4.17)$$

The step size is inversely proportional to Reynolds number for $\text{Re} > 2N$.

In case of backward differencing, the step size is

$$h_{\text{Max}} = 2/(\text{Modulus of } \lambda) \quad (4.18)$$

Figure 4.4 shows variations of step size with Reynolds number (Re) and the number of grid points (N). The figure shows that the step size de-

ORIGINAL PAGE IS
OF POOR QUALITY

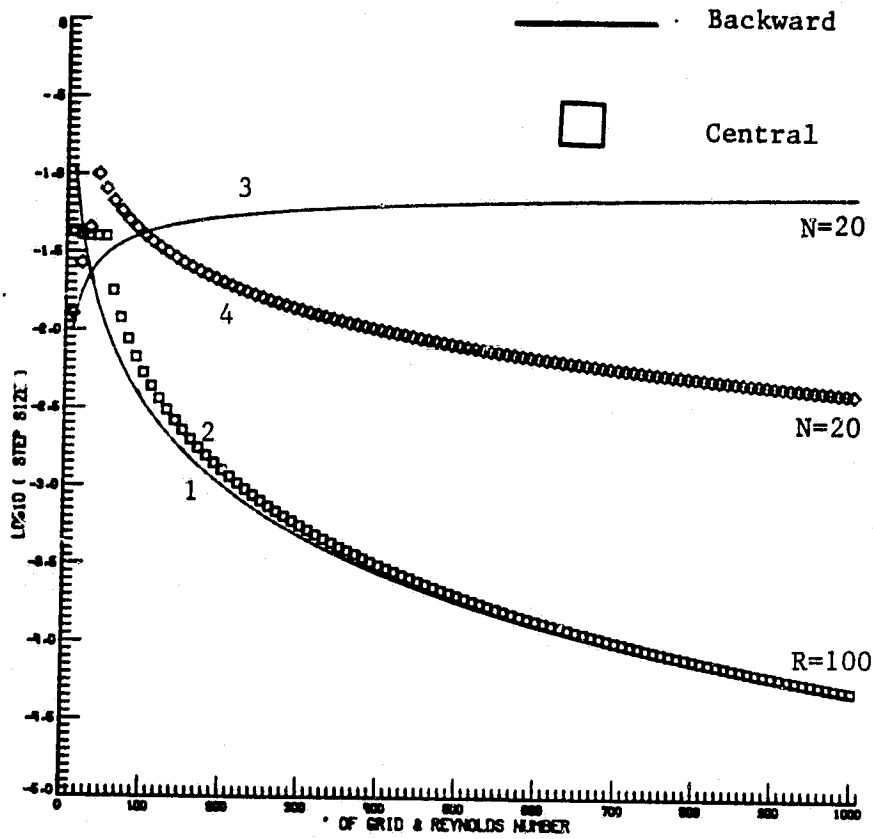


Fig. 4.4 Step size variation with Reynolds number and number of grids.

creases as the number of grid points increases (curves 1 and 2). This is compatible with the finite difference techniques [12]. On the same figure, step size is plotted versus Reynolds number. For backward differencing, the step size increases with increasing of the Reynolds number. The converse is true for central differencing.

For inviscid flow ($Re \rightarrow \infty$), forward differencing is inherently unstable. For central differencing, step size is zero which makes it impossible to integrate the equations. The step size for backward differencing is

$$h = 2/N \quad (4.19)$$

The step size is inversely proportional to the number of grid points; this result is similar to the result of viscous flow.

Chapter 5

BOUNDARY AND INITIAL CONDITIONS

For a particular flow problem, selection of proper boundary conditions depends upon the nature of the flow and the computational procedures employed. The application of certain conditions may cause numerical instability in the solution even though the flow is physically stable.

Equations (2.21) and (2.22) are parabolic-elliptic partial differential equations. The dependent variables in these equations should be defined by some relations along the boundaries. There are three general types of boundary conditions for a dependent variable and they can be stated as follows:

1. Specifying values of the dependent variables at the boundaries.
2. Specifying first or higher derivatives of the dependent variables at the boundaries.
3. Specifying algebraic relations which relate dependent variables to independent variables or to their first or higher order derivatives.

Two points should be noted in choosing the above conditions. First, the second condition cannot be applied at all boundaries because uniqueness considerations. Second, a combination of the above conditions can be applied to various parts of one boundary.

In the selection of boundary conditions, four important factors that should be considered are: convergence, stability, computer time, and above all, the physical justification. Extensive discussions of these factors are given by Roache [12].

For the confined flow geometry, Fig. 5.1a, there are four types of boundary conditions: inlet, outlet, wall, and symmetry. Whereas, in the driven cavity, Fig. 5.1b, there are two types of boundary conditions: wall and moving wall. Also, in each case, it is necessary to specify some initial conditions.

5.1 Inlet Condition

For problems involving duct flow, the inlet conditions are usually specified. Throughout this study, the inlet conditions are fixed. In general inlet velocity profile for duct flow is given by

$$U(r) = 1 - AI \cdot r^{NI}, \quad (5.1)$$

$$V(r) = 0.0 \quad (5.2)$$

The stream function is computed from Eqs. (2.11) and (2.12) by

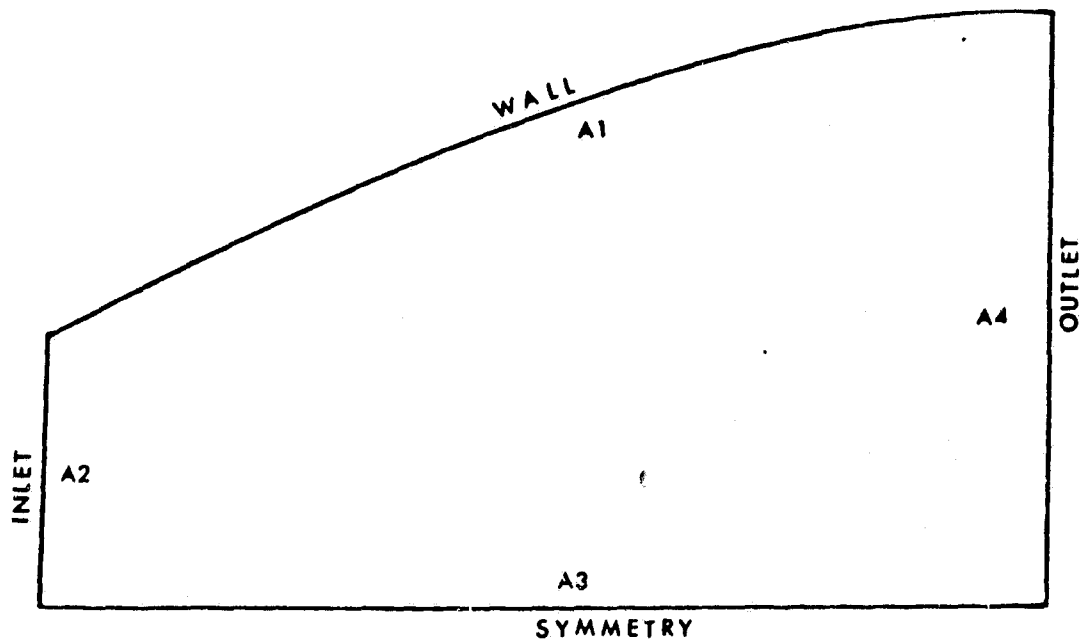
$$\psi(r) = \frac{r^{\delta+1}}{\delta+1} - AI \frac{r^{NI+\delta+1}}{NI+\delta+1} \quad (5.3)$$

The vorticity is computed similarly from Eq. (2.10) as

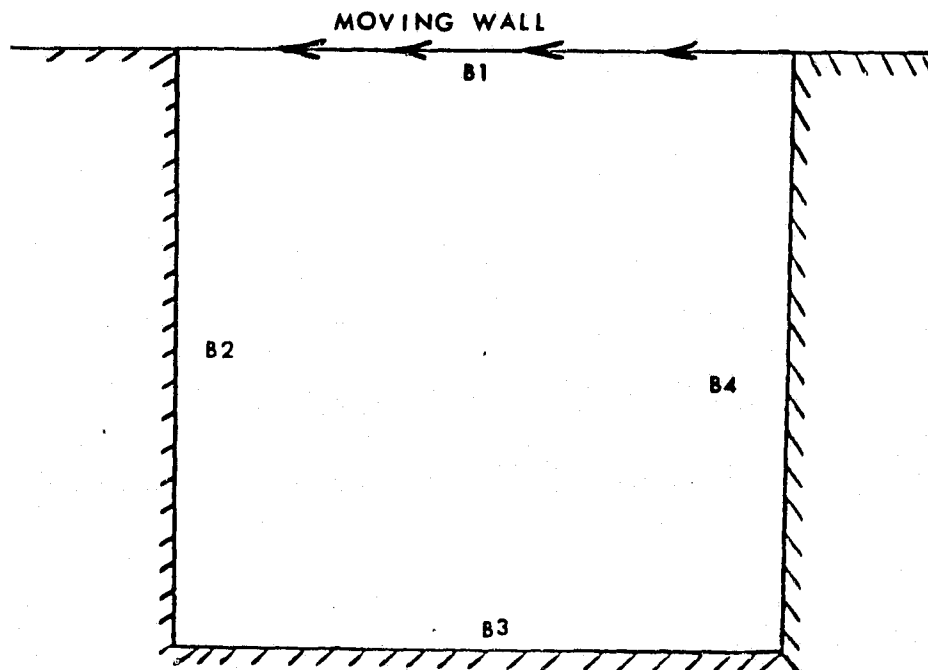
$$\omega = AI \cdot NI \cdot r^{NI-1} \quad (5.4)$$

In the preceding equations, NI and AI are the inlet distribution parameters and they can be selected to produce desired inlet conditions. For example, AI = 0 corresponds to a uniform distribution of velocity across the inlet; AI = NI = 1 corresponds to a linear distribution of

ORIGINAL PAGE IS
OF POOR QUALITY



(a) Confined flow geometry.



(b) Driven cavity geometry.

Fig. 5.1 Boundary conditions for various geometries.

inlet profile; $AI = 1$, $NI = 2$ corresponds to a parabolic inlet profile. In this study, a uniform inlet profile is selected for flows in pipe and parallel ducts, and a parabolic profile for flows in a curved-wall diffuser.

5.2 Outlet Condition

For flow between parallel plates and in pipes, the most realistic outlet condition would be no profile changes in the flow direction far from the entrance point; provided there is no change in the wall conditions. This makes it impossible to use realistic conditions for such cases. Roache [12] points out that numerical experiences show that catastrophic instability may be propagated upstream from the application of improper outlet conditions and this may destroy the solution completely.

The Reynolds number is an important criteria for selection of an outlet condition. For high Reynolds number flows, the derivatives with respect to flow direction are generally small compared to the derivatives with respect to normal direction. Therefore, the governing equations tend to be parabolic in nature (boundary-layer equations). In this case, the outlet condition has little effect on the solution. But, low Reynolds number flows require a physically well justifiable outlet condition. Generally, the outlet condition can be described to be fixed or to be time dependent. A fixed outlet condition is the easiest to apply from a computational viewpoint. For a fixed outlet condition, the velocity profile is given by

$$U(r) = U_{\max} (1 - AIr^{NI}) \quad (5.5)$$

$$\frac{\partial V}{\partial z} = 0 \quad (5.6)$$

The stream function and vorticity can be computed in the same way as described in Sec. 5.1. They are

$$\psi(r) = U_{\max} \left[\frac{r^{\delta+1}}{\delta+1} - AI \frac{r^{NI+\delta+1}}{NI+\delta+1} \right] \quad (5.7)$$

$$\omega(r) = U_{\max} AI \cdot NI \cdot r^{NI-1} \quad (5.8)$$

In the absence of suction and/or blowing, the stream function should be constant along the wall. This is given by

$$\{\psi(1)\}_{\text{Eq. (5.3)}} = \{\psi(r_2)\}_{\text{Eq. (5.7)}} \quad (5.9)$$

A combination of equations (5.7) and (5.9) results in

$$U_{\max} = \frac{1/(\delta+1) - AI/(NI + \delta + 1)}{r_2^{\delta+1}/(\delta+1) - AI r_2^{NO+\delta+1}/(NO+\delta+1)} \quad (5.10)$$

where r_2 is the outlet radius.

A fixed outlet condition is not suitable for separated flows or any flows with a viscous wake [12]. Paris and Whitaker [19] solved a confined flow using zero gradient conditions. This showed improvement in solution over specified conditions. Later, Thoman and Szewczyk [20] used physically less restricted conditions for the stream function and zero gradient on the vorticity as

$$\frac{\partial^2 \psi}{\partial z^2} = \frac{\partial \omega}{\partial z} = 0 \quad (5.11)$$

Briley (21) took a different approach by considering the following relation

$$\frac{\partial^2 \psi}{\partial z^2} = \frac{\partial^2 \omega}{\partial z^2} = 0 \quad (5.12)$$

A substitution of Eq. (5.12) into Eq. (2.14) results in

$$\omega = (1/r)^\delta \left[\frac{\partial^2 \psi}{\partial r^2} - \frac{\delta}{r} \frac{\partial \psi}{\partial r} \right] \quad (5.13)$$

Equations (5.12) and (5.13) represent two ways of computing vorticity at an outlet. This technique is referred to as maltreatment of outlet condition by Roache [22]. Throughout this study, Eq. (5.11) is considered for the outlet condition.

5.3 Wall Condition

An impermeable wall assumption allows the stream function to have a fixed value along a wall regardless of its geometry. The stream function may be computed from the inlet condition, Eq. (5.3),

$$\psi = \frac{1}{\delta + 1} - \frac{AI}{NI + \delta + 1} \quad (5.14)$$

The vorticity can be computed by applying Eq. (5.14) to Eq. (2.22), i. e.,

$$D_2 \psi_\eta + E_2 \psi_{\eta\eta} + F_2 = 0 \quad (5.15)$$

Also, zero velocity at the wall allows

$$\psi_\eta = 0 \quad (5.16)$$

Upon combining Eqs. (5.14) and (5.15), one obtains

$$\omega = - \frac{\eta^2}{r^\delta} \psi_{\eta\eta} \quad (5.17)$$

Equation (5.17) describes variations of vorticity along a horizontal wall. A similar expression can be derived for a vertical wall in the case of a driven cavity, i.e.,

$$\omega = - \frac{\xi^2 + \eta^2}{r} \psi_{\xi\xi} \quad (5.18)$$

Equation (5.17) is applied to the boundary A1 shown in Fig. 5.1a and to boundary B3 shown in Fig. 5.1b. Equation (5.18) is applied to boundaries B2 and B4 in Fig. 5.1b.

5.4 Symmetry Condition

Selection of a symmetry boundary condition depends on the nature of the flow. In this study, since there is no center body, the symmetry condition along the centerline requires that

$$\frac{\partial U}{\partial r} = 0 \quad (5.19)$$

$$V = 0 \quad (5.20)$$

By comparing Eqs. (5.18) and (2.12), it can be concluded that the stream function has a fixed value along the line of symmetry which can be chosen to be zero. Similarly, it can be concluded that the vorticity is zero along the line of symmetry.

5.5 Moving Wall Condition

In Fig. 5.1b, the B1 boundary moves with a uniform velocity $U=-1$. This means that the boundary can be chosen as a streamline. The value of the stream function can be selected to be zero to match with the value of the stream function at boundaries B2 and B4. Using uniform velocity at the boundary, Eq. (2.23) can be written as

$$\xi_r \psi_{\xi} + \eta_r \psi_{\eta} = -1 \quad (5.21)$$

By using the value of the stream function along the boundary ($\psi = 0$), this equation reduces to

$$\psi_{\eta} = -1/\eta_r \quad (5.22)$$

Vorticity can be obtained from Eq. (2.22) by using the value of the stream function along the boundary and Eq. (5.22), i. e.,

$$\omega = D_2/\eta_r - E_2 \psi_{\eta\eta} \quad (5.23)$$

The second derivative of the stream function can be approximated (second order) by

$$\psi_{\eta\eta} = \psi_{N+IN} - 2\psi_N + \psi_{N-IN} \quad (5.24)$$

Also, the first derivative of the stream function can be approximated (third order) by

$$\psi_{\eta} = (2\psi_{N+IN} + 3\psi_N - 6\psi_{N-IN} + \psi_{N-2IN})/6 = -1/\eta_r \quad (5.25)$$

The combination of Eqs. (5.24) and (5.25) results in

$$\psi_{\eta\eta} = (-6/\eta_r + 8\psi_{N-IN} - \psi_{N-2IN} - 7\psi_N)/2. \quad (5.26)$$

Equation (5.26) is a second order accurate equation [23].

A combination of Eqs. (5.23) and (5.26) results in

$$\omega = D_2/\eta_r + E_2 (6/\eta_r - 8\psi_{N-IN} + \psi_{N-2IN} + 7\psi_N)/2.0 \quad (5.27)$$

A similar approach has been employed for evaluating the vorticity at the stationary wall boundaries.

5.6 Initial Conditions

In computational fluid dynamics, the initial conditions usually correspond to a real initial situation for a transient problem or, as a rough guess, for a steady state problem. In practice, initial conditions are obtained from experiments, empirical relations, or approximate theories. The initial conditions used in the determination of the steady state solution should have no significance in the steady-state solution of incompressible flows [12], otherwise the solution is not unique.

Generally, there are two kinds of initial conditions. In the first one, an impulse motion starts from the rest, and in the second kind, the flow has the same initial motion everywhere except the boundaries. In the present study, the entire flow-field is initially set equal to the inlet condition for the internal flows. For the case of driven cavity, the stream function and vorticity are initially set equal to zero in the entire flow-field.

Chapter 6

GRID GENERATION TECHNIQUES

It is highly desirable to solve partial differential equations in a rectangular box with uniform grid spacings [25-27]. This is especially true in fluid dynamics where the governing equations are complex. Ideally, a physical domain should be transformed to a computational domain, where the physical boundaries map into the boundaries of a rectangle. This transformation has certain advantages. In the first place, the boundaries can be represented more accurately. Secondly, it allows better resolution in regions where rapid changes occur, such as boundary layers, shocks, and separated flows. Above all, computer codes which are applicable to any geometry can be written without the need of special procedures for the boundaries. The disadvantages are that the convergence, stability, and stiffness characteristics of the equations are affected. Also, the transformed equations are more complex than the original equations. The transformed governing equations contain the rate of change of the computational coordinates with respect to the physical coordinates. These derivatives are computed from the relations of the physical grid to the computational grid. There are, generally, three approaches for grid generations: classical technique (conformal mapping) [24], differential methods [25], and algebraic methods [26].

The classical technique requires the use of complex functions to define the mapping which is extremely difficult for arbitrary geometries. But, conformal mapping has the advantage of minimizing the number of terms in the transformed equations. The algebraic and differential methods for grid generation are outlined in the following sections.

6.1 Algebraic Method

In the algebraic method an explicit functional relationship between the computational domain and the physical domain is determined. The computational domain is rectangular and has a uniform grid distribution. The physical domain is defined by

$$z = z(\xi, \eta) \quad (6.1)$$

$$r = r(\xi, \eta) \quad (6.2)$$

A requirement of boundary-fitted coordinate systems is that the boundaries of physical domain map to the boundaries of the computational domain. That is,

$$z_1 = z_1(\xi, 0) = z_1(\xi) \quad (6.3)$$

$$\eta_1 = \eta_1(\xi, 0) = \eta_1(\xi) \quad (6.4)$$

$$z_2 = z_2(\xi, 1) = z_2(\xi) \quad (6.5)$$

$$\eta_2 = \eta_2(\xi, 1) = \eta_2(\xi) \quad (6.6)$$

Equations (6.1) and (6.2) can be rewritten using Eqs. (6.3) through (6.6) as

$$z = z(\xi, \eta) = z(z_1, z_2, \eta) \quad (6.7)$$

$$r = r(\xi, \eta) = r(\eta_1, \eta_2, \eta) \quad (6.8)$$

The explicit forms of Eqs. (6.7) and (6.8) can be written as a simple parametric linear or cubic polynomials as [26]

Linear:

$$z = z_2(\xi)\eta + z_1(\xi)(1-\eta) \quad (6.9)$$

$$r = r_2(\xi)\eta + r_1(\xi)(1-\eta) \quad (6.10)$$

Cubic:

$$z = z_1(\xi) f_1(\eta) + z_2(\xi) f_2(\eta) + \frac{dz^1(\xi)}{d\eta} f_3(\eta) + \frac{dz_2(\xi)}{d\eta} f_4(\eta) \quad (6.11)$$

$$r = r_1(\xi) f_1(\eta) + r_2(\xi) f_2(\eta) + \frac{dr_1(\xi)}{d\eta} f_3(\eta) + \frac{dr_2(\xi)}{d\eta} f_4(\eta) \quad (6.12)$$

In Eqs. (6.11) and (6.12), the f 's are the blending functions and are defined as

$$f_1 = 2\eta^3 - 3\eta + 1 \quad (6.13)$$

$$f_2 = -2\eta^3 + 3\eta \quad (6.14)$$

$$f_3 = \eta^3 - 2\eta^2 + \eta \quad (6.15)$$

$$f_4 = \eta^3 - \eta^2 \quad (6.16)$$

Equations (6.9) through (6.12) are called connecting functions. If $\bar{\xi}$ and $\bar{\eta}$ are the computation coordinate functions, then $\bar{\xi}(\xi)$ and $\bar{\eta}(\eta)$ can be defined to produce a desired grid spacing distribution. That is

$$\bar{\xi} = \bar{\xi}(\xi) \quad , \quad 0 \leq \xi < 1 \quad , \quad 0 \leq \bar{\xi} < 1 \quad (6.17)$$

$$\bar{\eta} = \bar{\eta}(\eta) \quad , \quad 0 \leq \eta < 1 \quad , \quad 0 \leq \bar{\eta} < 1 \quad (6.18)$$

For example, contracting the physical grids towards one boundary can be

accomplished by using the following function

$$\bar{\eta} = \frac{e^{K\eta-1}}{e^{K-1}} \quad (6.19)$$

where K is a stretching parameter which determines the location and degree of concentration.

This method (i.e., the algebraic method) requires relatively few computations.

6.2 Differential method

If the computational coordinates $\xi(z,r)$ and $\eta(z,r)$ are harmonic then the Jacobian does not vanish [27]. This allows a computation of ξ and η from an elliptic system (Laplace's equation), i.e.,

$$\nabla^2 \xi = 0 \quad (6.20)$$

$$\nabla^2 \eta = 0 \quad (6.21)$$

The spacing of the coordinate lines can be controlled by adding inhomogeneous term to the right sides of Eqs. (6.20) and (6.21) as

$$\nabla^2 \xi = P(\xi, \eta) \quad (6.21a)$$

$$\nabla^2 \eta = Q(\xi, \eta) \quad (6.21b)$$

In Eqs. (6.21a) and (6.21b), η and ξ are known, and the unknowns are z and r . In order to be able to solve for z and r , the dependent variables of Eqs. (6.20) and (6.21) should be interchanged. Thus,

$$\alpha z_{\xi\xi} - 2\beta z_{\xi\eta} + \gamma z_{\eta\eta} = -J^2 [Pz_{\xi} + Qz_{\eta}] \quad (6.22)$$

$$\alpha r_{\xi\xi} - 2\beta r_{\xi\eta} + \gamma r_{\eta\eta} = -J^2 [Pr_{\xi} + Qr_{\eta}] \quad (6.23)$$

where

$$\alpha = z_{\eta}^2 + r_{\eta}^2 \quad (6.24a)$$

$$\beta = z_{\xi} z_{\eta} + r_{\eta} r_{\xi} \quad (6.24b)$$

$$\gamma = z_{\xi}^2 + r_{\xi}^2 \quad (6.24c)$$

$$J = z_{\xi} r_{\eta} - z_{\eta} r_{\xi} \quad (6.24d)$$

There are four boundary conditions for Eqs. (6.22) and (6.23). The quantities P and Q are the forcing functions which are selected to have a desired grid distribution and orthogonality at the boundaries [27]. The disadvantage of this method is that it is inefficient compared to the algebraic method.

Chapter 7

PHYSICAL APPLICATIONS

This study investigates the validity and viability of the method of lines for solutions of the Navier-Stokes equations with arbitrary boundary geometry and grid spacing. For incompressible viscous flows, the pertinent equations are derived in two-dimensional and axisymmetric coordinate systems, Eqs. (2.13) -(2.15). These equations are transformed from the physical domain with arbitrary boundaries and grid spacings to a rectangular computational domain with uniform grid spacings. The resulting equations, Eqs.(2.21) and (2.22), are solved numerically. The method of lines is used to solve the vorticity equation, Eq. (2.22), and the successive overrelaxation technique is used for solving the stream function equation, Eq. (2.21). Boundary conditions at a solid stationary wall are no-slip conditions which corresponds to a fixed stream function and requires that the vorticity be computed from the stream function by Eqs. (5.17) and (5.26). For the internal flow computation, the stream function and vorticity are equal to zero along the line of symmetry. The inflow boundary condition is kept fixed throughout this study. The outflow condition is used to enforce no-change in the stream function and vorticity with respect to flow direction, Eq. (5.11). In the case of the driven cavity, the vorticity at the moving wall is computed from Eq. (5.28). For internal flow, the initial conditions are the inflow conditions for the entire domain, and no flow in the case of the driven cavity. Grid

distributions are generated by the algebraic method which makes it possible to handle any boundary geometries [26]. Specific solutions are obtained for internal flows (pipe, parallel plate and curved wall diffusers) and a driven cavity. These problems are discussed briefly in this chapter.

7.1 Internal Flows

The entrance regions of ducts are used usually to compare numerical procedures, because of the availability of analytical solutions. Most of these solutions are based on parabolic forms of Navier-Stokes equations which are called boundary-layer equations. Assumption of the boundary layer (neglecting the axial diffusion) makes it possible to obtain analytical solutions [28-31].

Vrentas et al. [32] investigated the effects of axial diffusion of vorticity on flow development in circular ducts. It was concluded that at very low Reynolds numbers ($Re < 20$), the axial diffusion causes the velocity development to be spread out in the downstream region, and this results in a larger entrance length than that predicted by the boundary-layer analysis. It was also concluded that the converse is true for $Re > 20$. The flow in parallel ducts may, in general, be divided into three regions (Fig. 7.1). Region I, is a region of potential flow. This flow interacts with region II which is a region of boundary-layer flow. The third region (region III) is the region of fully-developed flow. Using these concepts, Schlichting [28] obtained an approximate solution by using Blasius' solution for the inlet regions between parallel ducts and a perturbation of the fully-developed solution in the region far from the entrance. The solution for the intermediate regions was obtained by patching together the upstream and

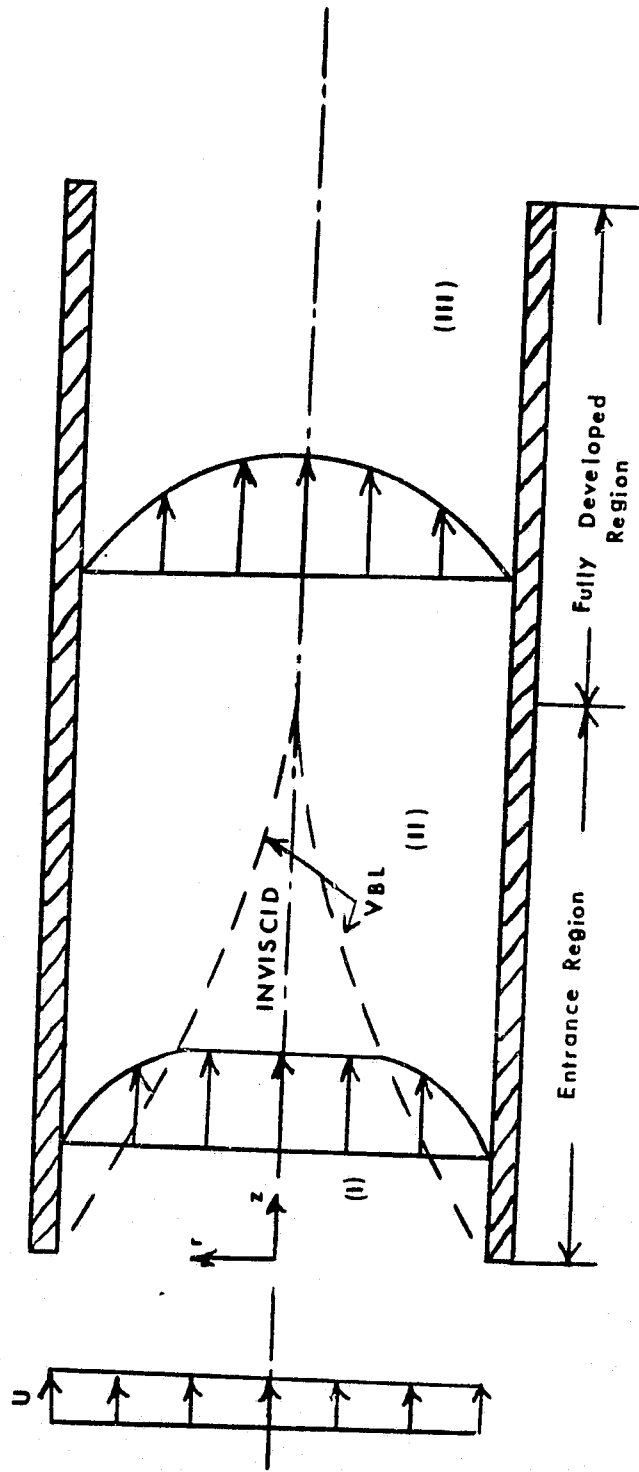


Fig. 7.1 Physical model for duct flow.

downstream solutions. A similar approach was implemented by Atkins and Goldstein [33] for a circular tube. Later, Van Dyke [31] improved Schlichting's solution by using more terms in the perturbation expansion. Another common method is the linearization of the convective term in the boundary-layer equations; this allows the velocity to be continuous along the axial coordinate. Using this concept, Sparrow et al. [30] developed solutions for circular tubes and parallel plates using boundary-layer equations. In the present study, results obtained from the method of lines are compared with results of Sparrow et al. [30].

In the case of curved-wall diffusers, the outer wall geometry is based on the following equation:

$$r = \left\{ 1 + (r_2 - 1) \frac{X}{L} \left[1 + \bar{\alpha} \left(1 - \frac{X}{L} \right) \right] \right\} H(X-L) + X H(L-X)$$

where

(7.1)

$$r_2 = L \tan \theta + 1$$

Figure 7.2 shows a typical curved-wall diffuser geometry. It is a bell-type diffuser for $\bar{\alpha} > 0$ and a trumpet type diffuser for $\bar{\alpha} < 0$. The value of $\bar{\alpha}$ has been set equal to unity for the present study. By using the method of lines, solutions are obtained for different diffuser angles (θ) and for a Reynolds number of 200.

7.2 Driven Cavity

The flow in a driven cavity has been used as a test case for evaluating the numerical procedures for solving the Navier-Stokes equations. It serves as an example of closed stream lines which represent

ORIGINAL PAGE IS
OF POOR QUALITY

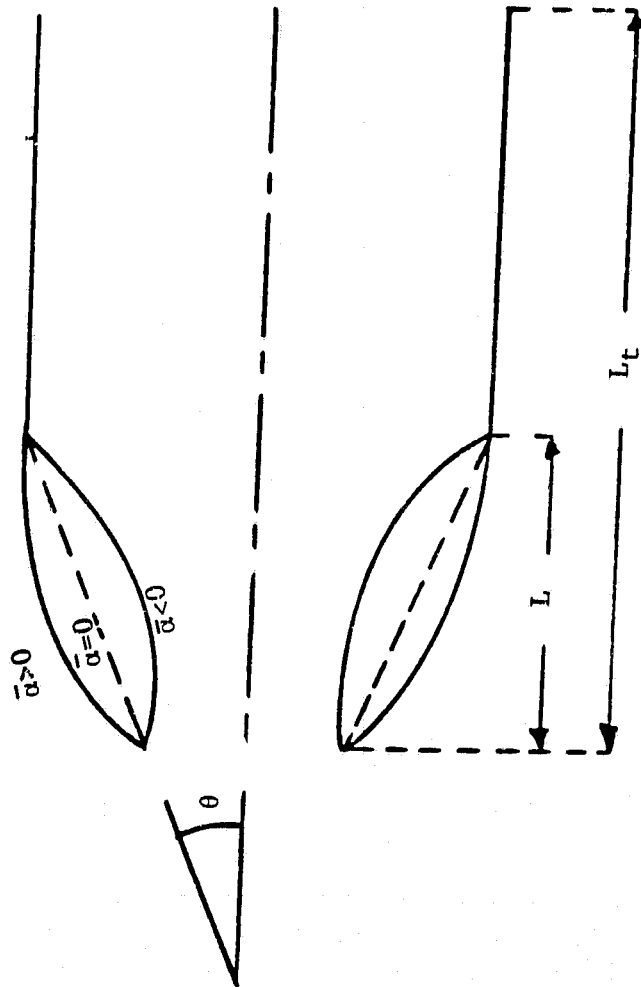


Fig. 7.2 Curved-wall diffuser geometry.

interesting characteristics such as vortex development in the core and boundary-layer development on the walls of the cavity.

Kawaguti [34] performed one of the earliest calculations for flow in a driven cavity and satisfactory results were obtained with Reynolds number up to 64. Later, Burggraf [35] obtained solutions for Reynolds numbers up to 400. An underrelaxation method was used to solve the governing equations, and a relaxation factor of 0.4 was used for a Reynolds number of 400. Burggraf was not successful in obtaining solutions for higher Reynolds numbers. This may be due partially to the form of the governing equations (non-conservative form) used. Bozeman [36] solved the same problem using the conservative form of the Navier-Stokes equations. Solutions were obtained successfully up to Reynolds numbers of 1000. Bozeman used a strongly implicit procedure which is unconditionally stable. Smith and Kidd [11] obtained solutions up to a Reynolds number of 5000 by solving the vorticity equation using alternating-direction implicit (ADI) methods and the stream function equation by the Buneman direct method (BDM). Using the method of lines, Kurtz et al. [8] were able to obtain solutions up to Reynolds numbers of 50,000. In this study, solutions are obtained for three Reynolds numbers (100, 1000, and 10000) with two different 16x16 grid distributions.

Chapter 8

RESULTS AND DISCUSSION

By using the formulation and numerical procedure discussed in the preceding chapters, solutions are obtained for flow between parallel plates, circular pipes, curved-wall diffusers, and in a driven cavity. Non-conservative forms of the governing equations are used for the entire internal flow computations.

Figure 8.1 shows the 20x20 grid distribution which is used for computing the flow field between parallel plates and in pipes. The grids are concentrated near the walls and the entrance point where rapid changes occur.

For a Reynolds number of 200, Figs. 8.2 and 8.3 show velocity, stream function and vorticity distributions for flow between parallel plates and in a pipe, respectively. Velocity profiles are compared with those obtained by Sparrow et al. [30], and are found to be in good agreement except in the vicinity of the entrance point. This discrepancy may be due to the fact that Sparrow's results are based on the boundary-layer assumptions. There is a sharp drop in the stream function in the vicinity of the entrance point which indicates a rapid flow development in this region. This sharp drop corresponds to a sharp change in vorticity which can be observed in Figs. 8.2c and 8.3c. Similar results are obtained for a Reynolds number of 1000 and these are illustrated in Figs. 8.4 and 8.5 for flow between parallel plates and in a pipe, respectively.

ORIGINAL PAGE IS
OF POOR QUALITY

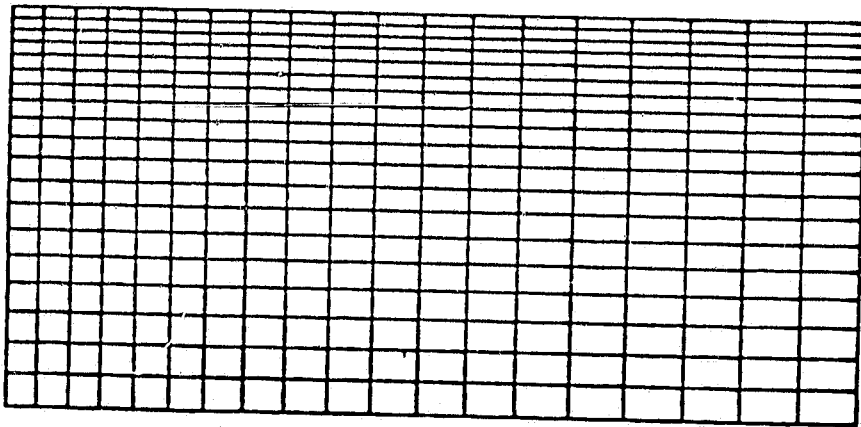
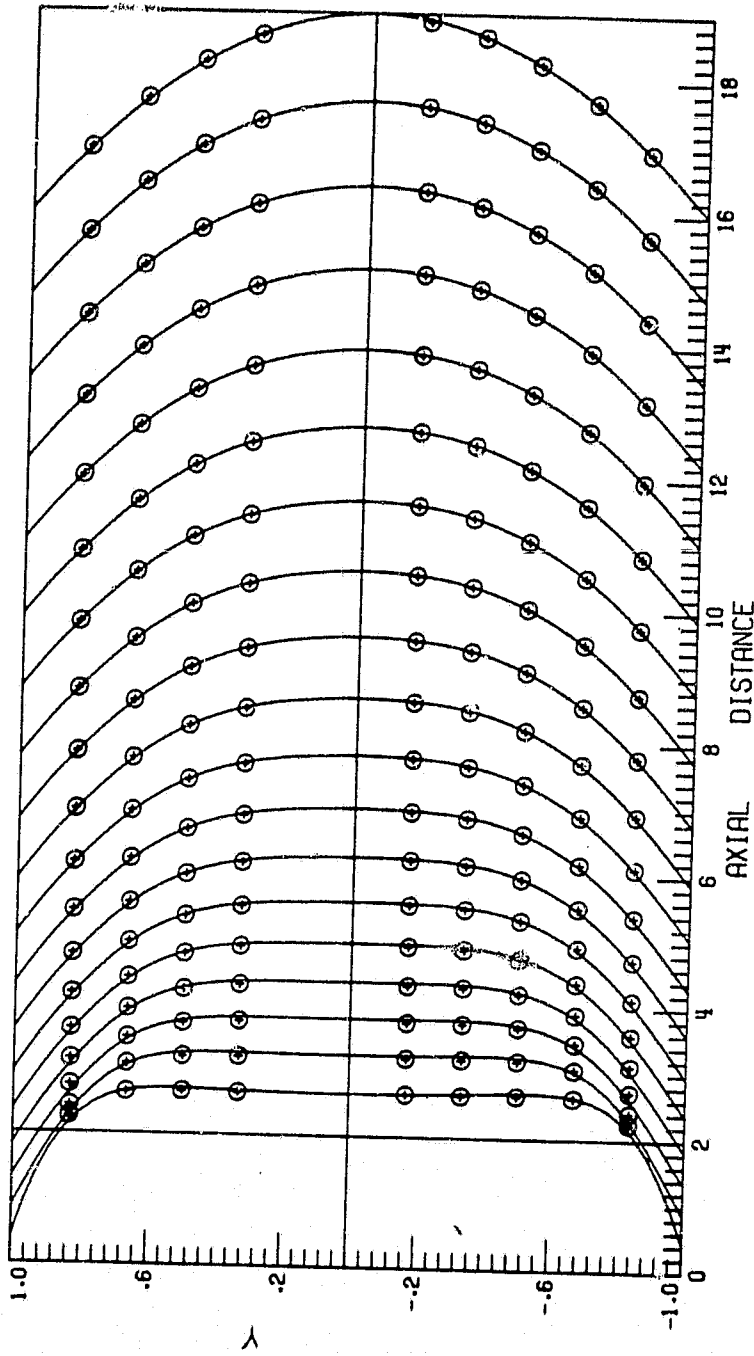


Fig. 8.1 Grid distribution for parallel plates and pipe.

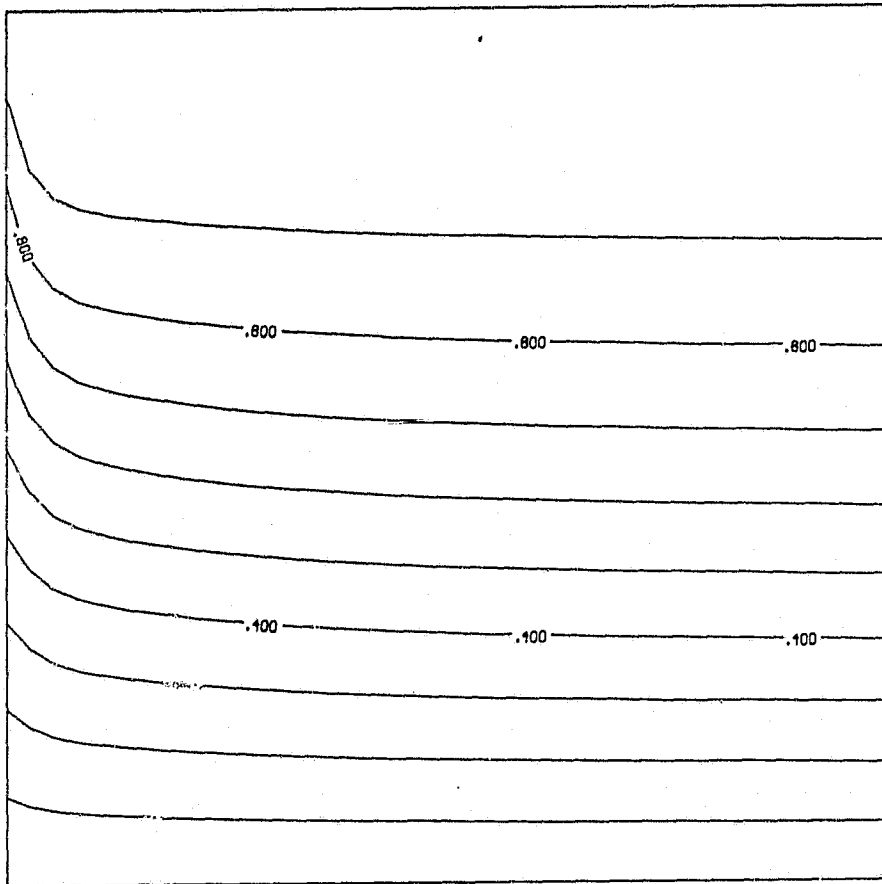


⊗ Ref. 30

— Present study

Fig. 8.2a Velocity distribution for flow between parallel plates, $Re = 200$.

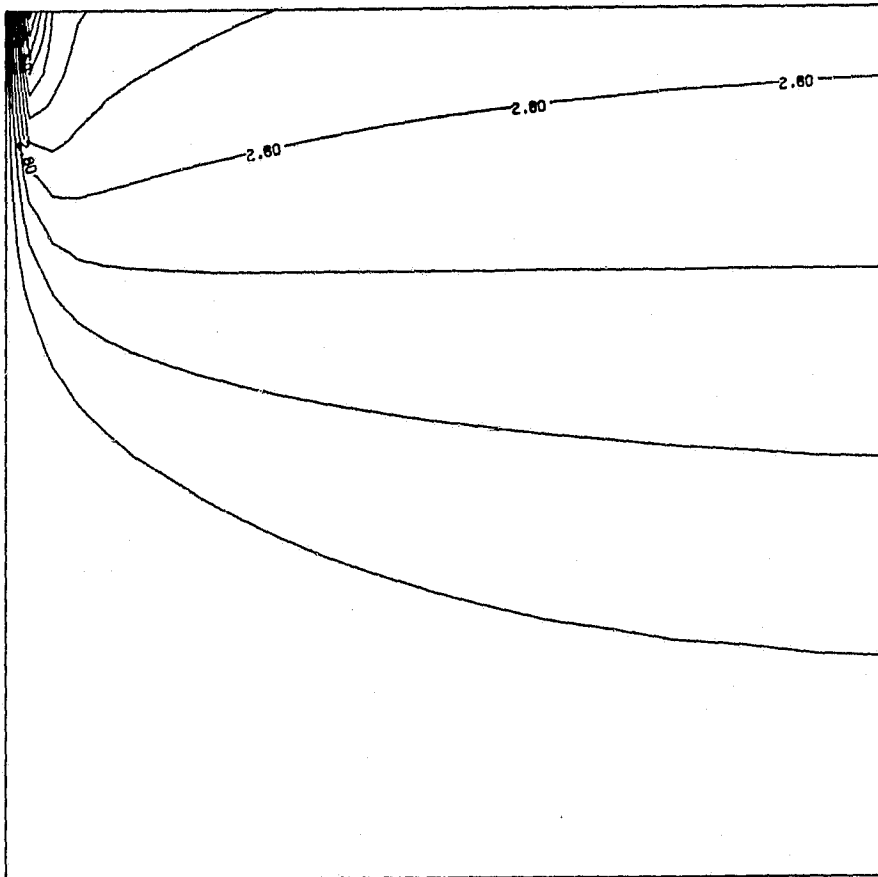
ORIGINAL PAGE IS
OF POOR QUALITY



CONTOUR FROM 0. TO 1.0000
CONTOUR INTERVAL IS .10000E+00

Fig. 8.2b Stream function contours for flow between parallel plates, $Re = 200$.

ORIGINAL PAGE IS
OF POOR QUALITY



CONTOUR FROM 0. TO 7.7000
CONTOUR INTERVAL IS .70000

Fig. 8.2c Vorticity contours for flow between parallel plates,
 $Re = 200$.

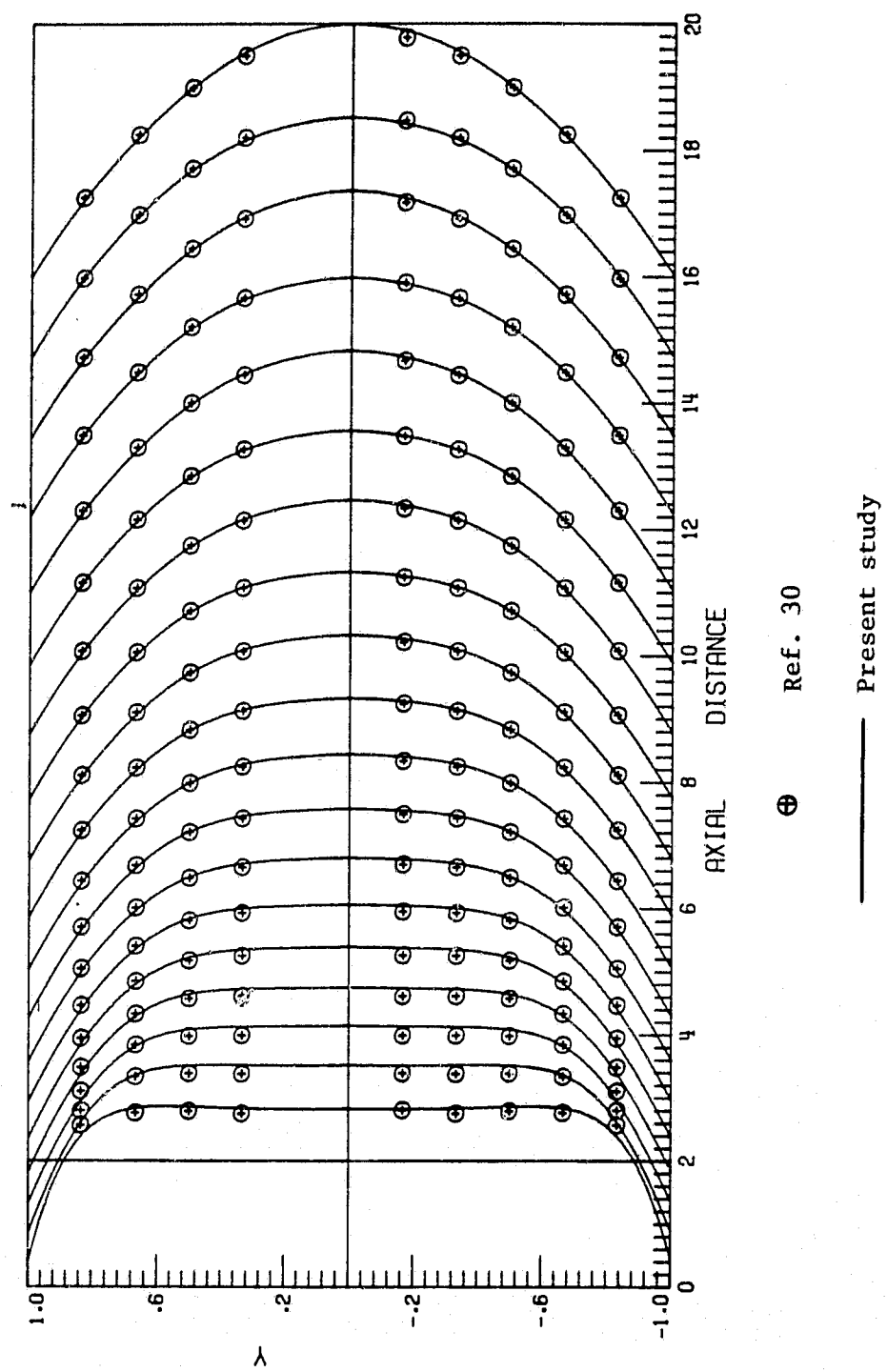
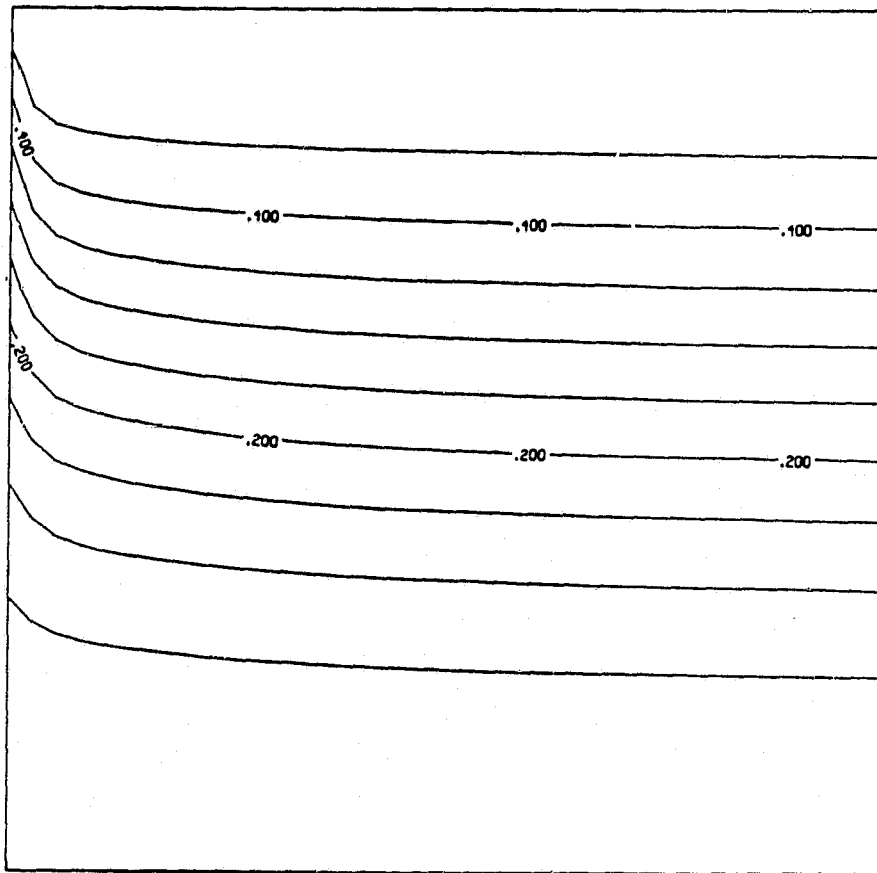


Fig. 8.3a Velocity distribution for pipe flow, $Re = 200$.

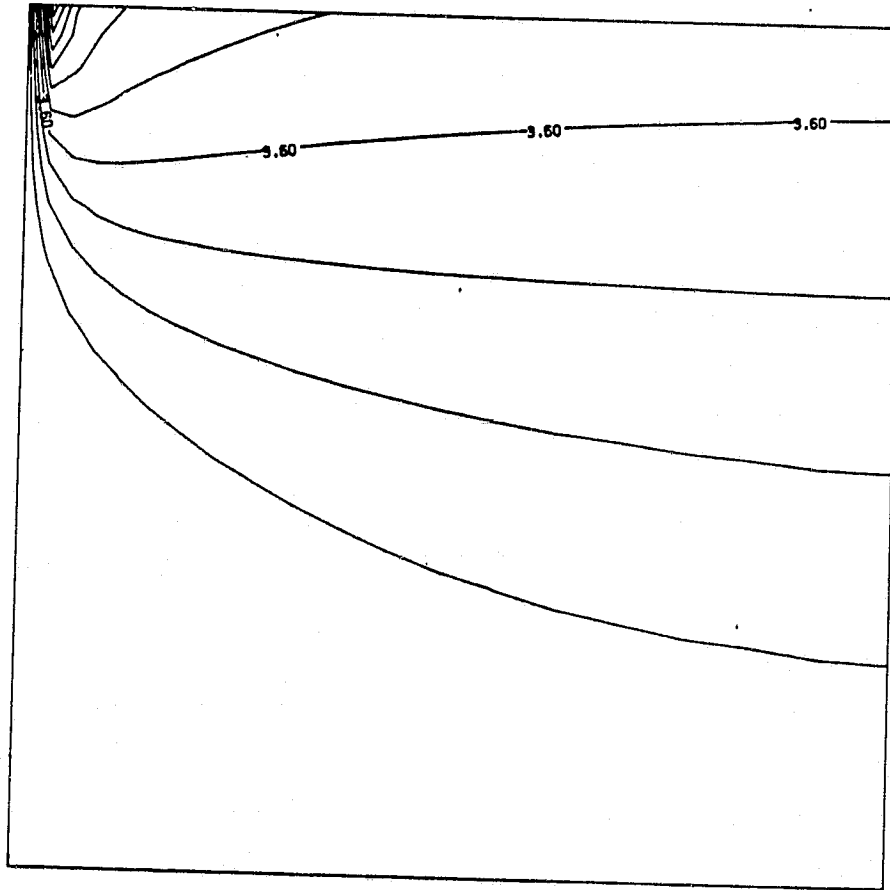
ORIGINAL PAGE IS
OF POOR QUALITY



CONTOUR FROM 0. TO .50000
CONTOUR INTERVAL IS .50000E-01

Fig. 8.3b Stream function contours for pipe flow, $Re = 200$.

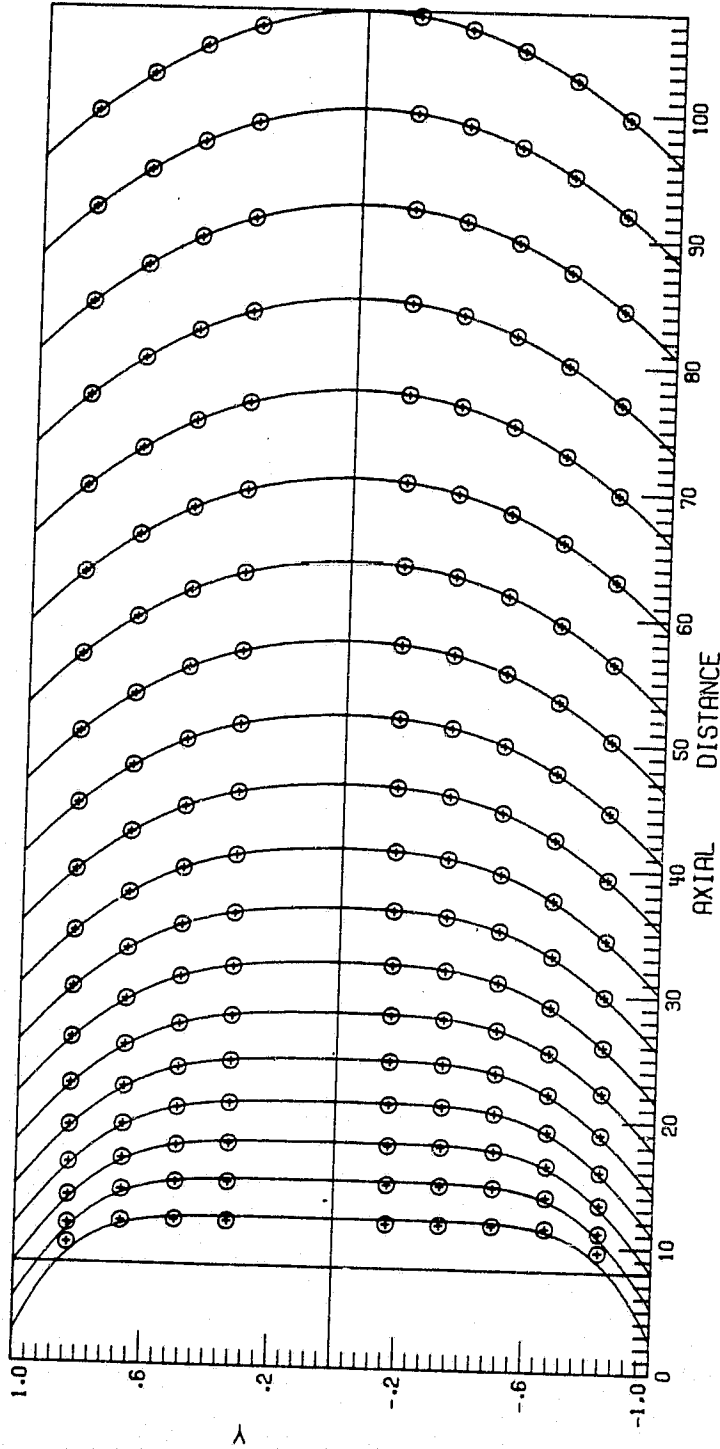
ORIGINAL PAGE IS
OF POOR QUALITY



CONTOUR FROM 0. TO 9.0000
CONTOUR INTERVAL IS .90000

Fig. 8.3c Vorticity distribution for pipe flow, $Re = 200$.

ORIGINAL PAGE IS
OF POOR QUALITY

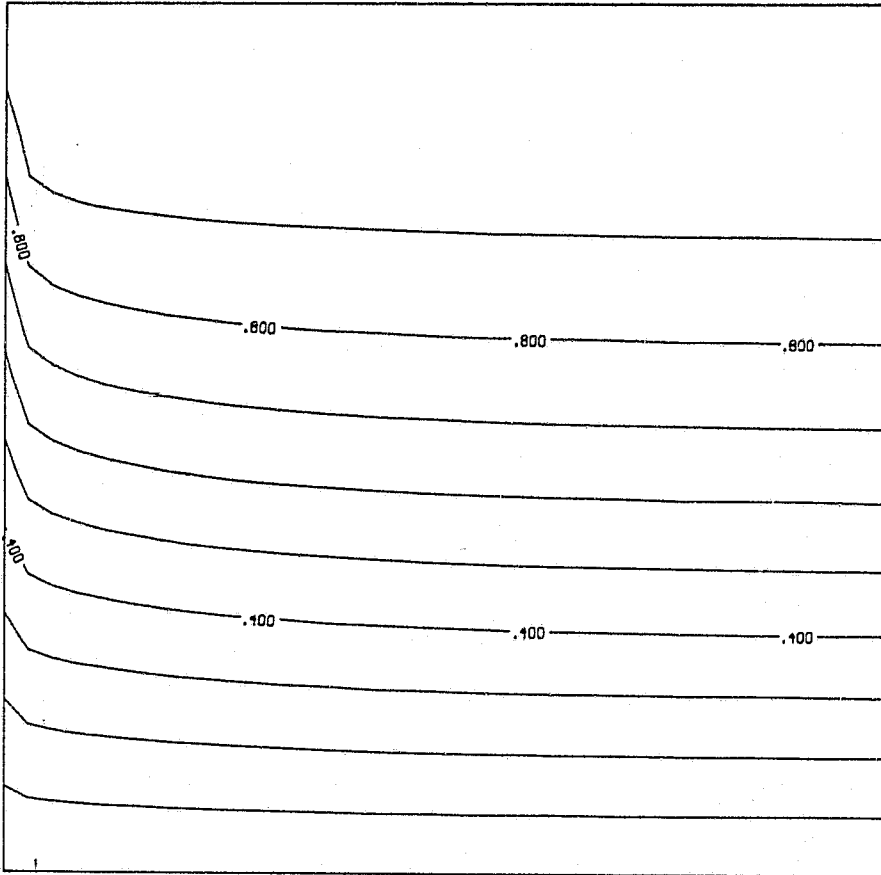


⊕ Ref. 30

— Present study

Fig. 8.4a Velocity distribution for flow between parallel plates, $Re = 1,000$.

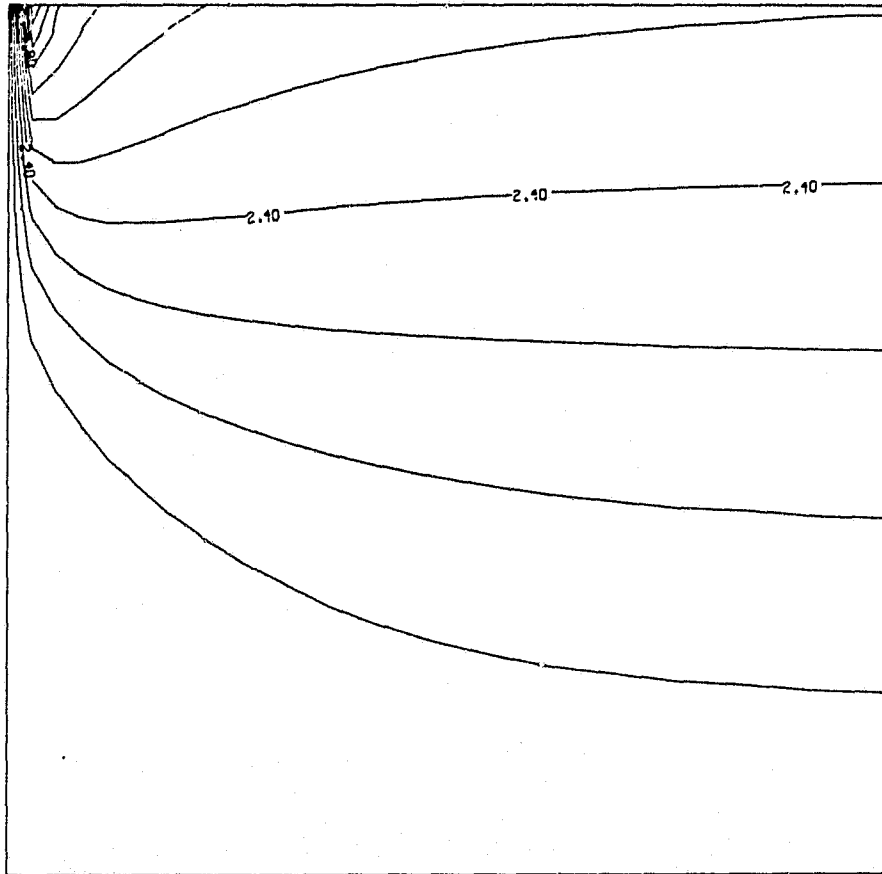
ORIGINAL PAGE 19
OF POOR QUALITY



CONTOUR FROM 0. TO 1.0000
CONTOUR INTERVAL IS .10000E+00

Fig. 8.4b Stream function contours for flow between parallel plates, $Re = 1,000$.

ORIGINAL PAGE IS
OF POOR QUALITY



CONTOUR FROM 0. TO 6.0000
CONTOUR INTERVAL IS .60000

Fig. 8.4c Vorticity contours for flow between parallel plates,
 $Re = 1,000$.

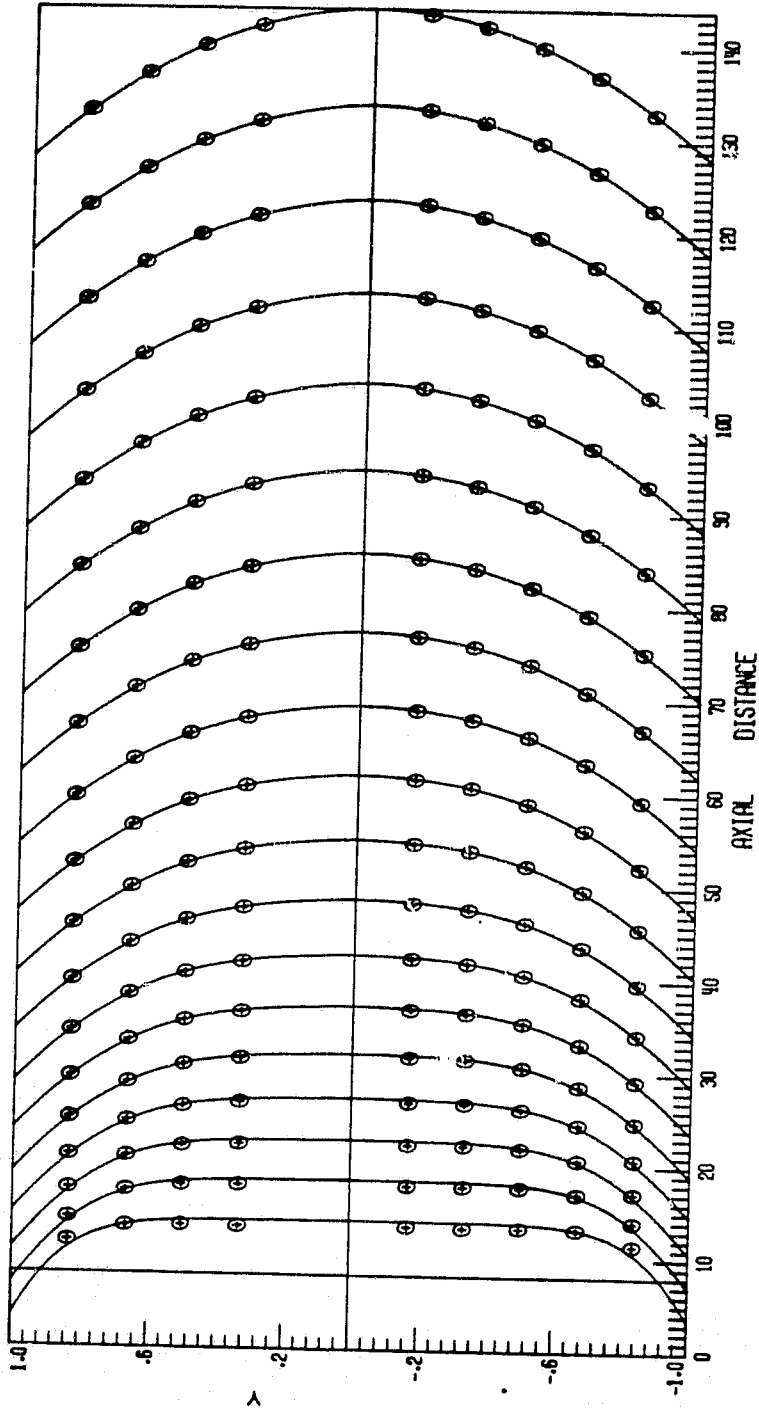
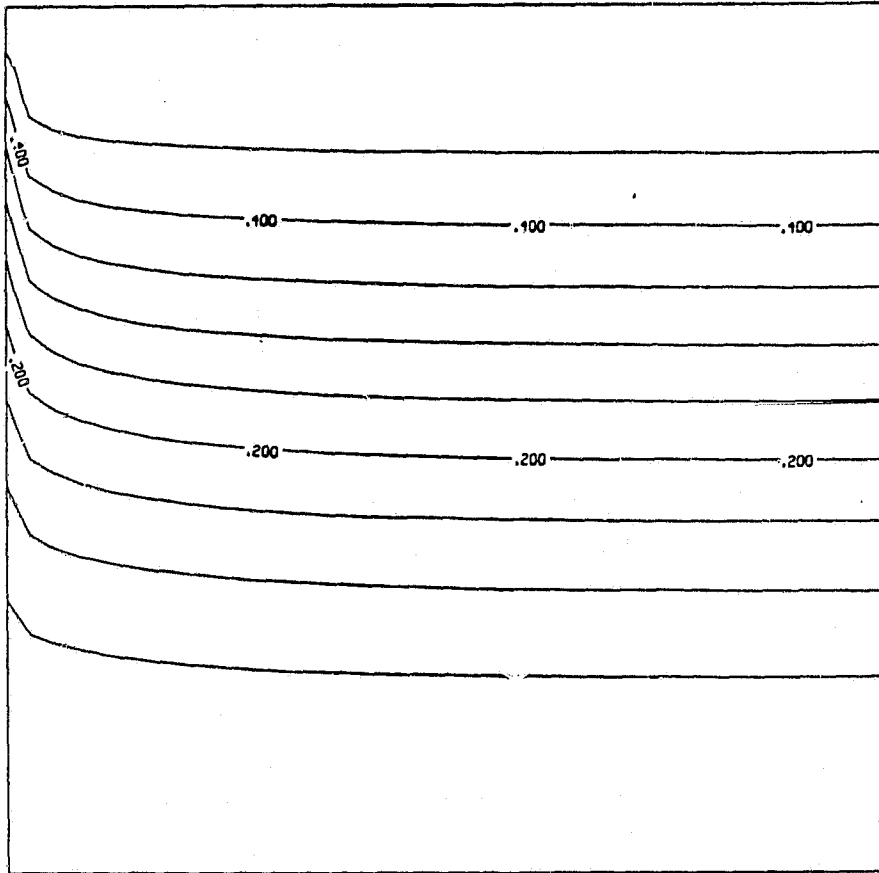


Fig. 8.5a Velocity distribution for pipe flow, $Re = 1,000$.

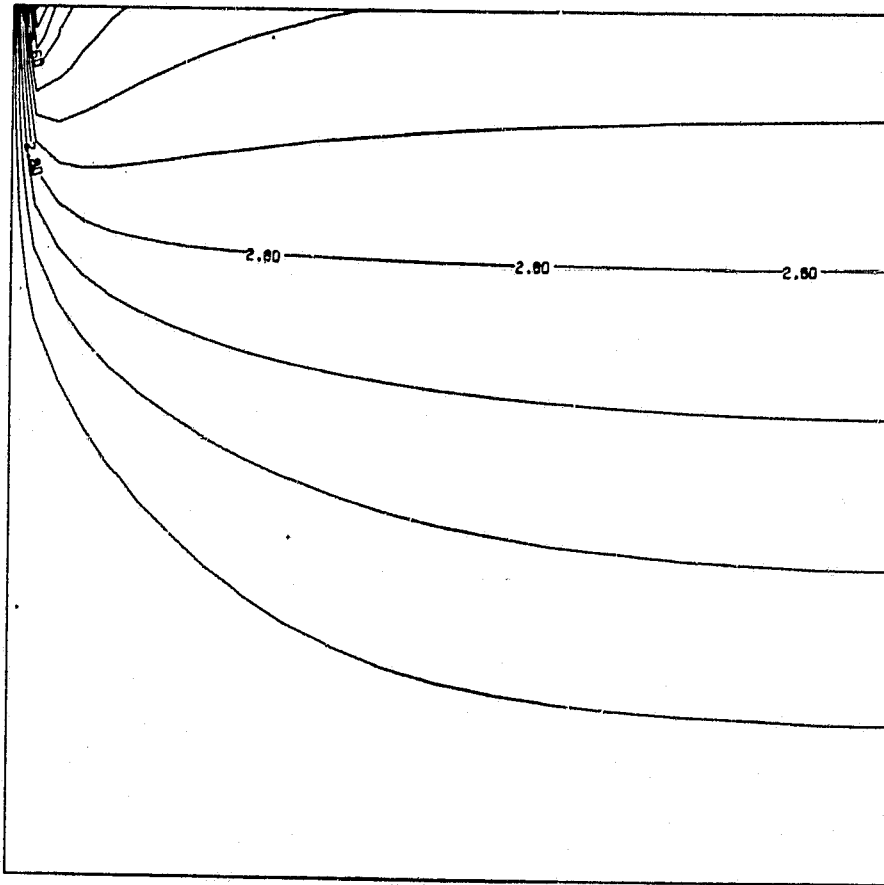
ORIGINAL PAGE IS
OF POOR QUALITY



CONTOUR FROM 0.
CONTOUR INTERVAL IS TO .50000
.50000E-01

Fig. 8.5b Stream function contours for pipe flow, $Re = 1,000$.

ORIGINAL PAGE IS
OF POOR QUALITY



CONTOUR FROM 0.
CONTOUR INTERVAL IS TO 7.7000
.70000

Fig. 8.5c Vorticity contours for pipe flow, $Re = 1,000$.

Figure 8.6 shows a 20x20 grid distribution for a five-degree curved-wall diffuser. Again, the grid is concentrated near the entrance point and wall region for capturing the boundary layer development and separation. Figure 8.7 shows the velocity profiles, stream function and vorticity distributions for a Reynolds number of 200. The results show no indication of separation. The next case studied is a ten-degree curved-wall diffuser. The grid distribution for this case is shown in Fig. 8.8, and the results shown in Fig. 8.9 clearly indicate that a separation occurs in this case.

Figure 8.10 shows a uniform 16x16 grid distribution for a driven cavity. Figure 8.11 shows the the stream function and vorticity distributions for Reynolds number of 100. These results are obtained using the non-conservative form of the Navier-Stokes equations with a uniform grid distribution. The results are in good agreement with the results obtained by other investigators [8, 11, 23, 35-37]. For a Reynolds number of 1000, the solution does not converge if the non-conservative form of the governing equation is used. For higher Reynolds numbers, therefore, the conservative form of the governing equations, Eqs. (2.15), are used to obtain further results. Figure 8.12 shows the stream function and vorticity distributions for a Reynolds number of 1000. The results are in good agreement with Kurtz et al. [8], Smith et al. [11], Ghia et al. [23], Bozeman [36], and Schreiber and Keller [37]. Ghia and Schreiber have used over 10^4 grid points. Figure 8.13 shows the stream function and vorticity distributions for Reynolds number of 10,000. The results are in good agreement with the results of Kurtz et al. [8], Ghia et al. [23] and Schreiber and Keller [37]. These results suggest that the high Reynolds number

ORIGINAL PAGE IS
OF POOR QUALITY

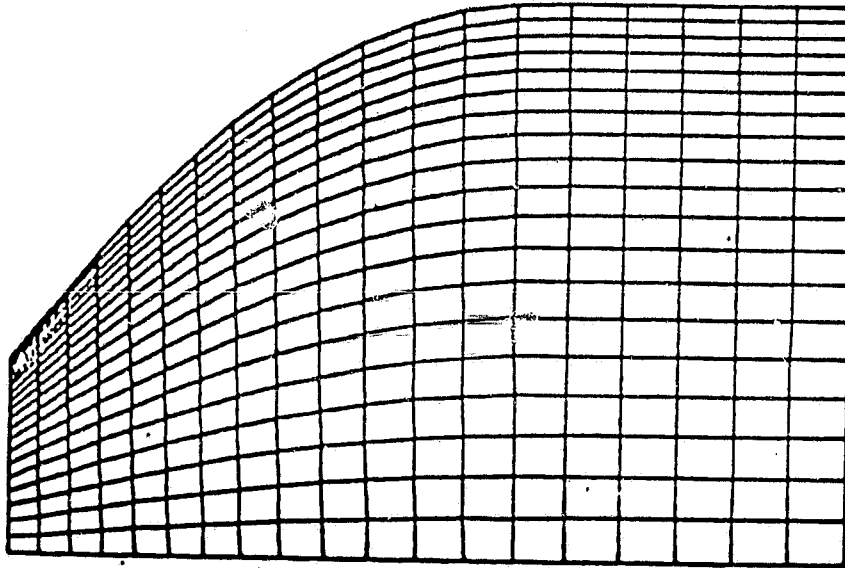


Fig. 8.6 Grid distribution for a bell-type diffuser,
 $\bar{\alpha} = 1$, $\theta = 5$, $L = 20$, $L_t = 32$.

ORIGINAL PAGE IS
OF POOR QUALITY

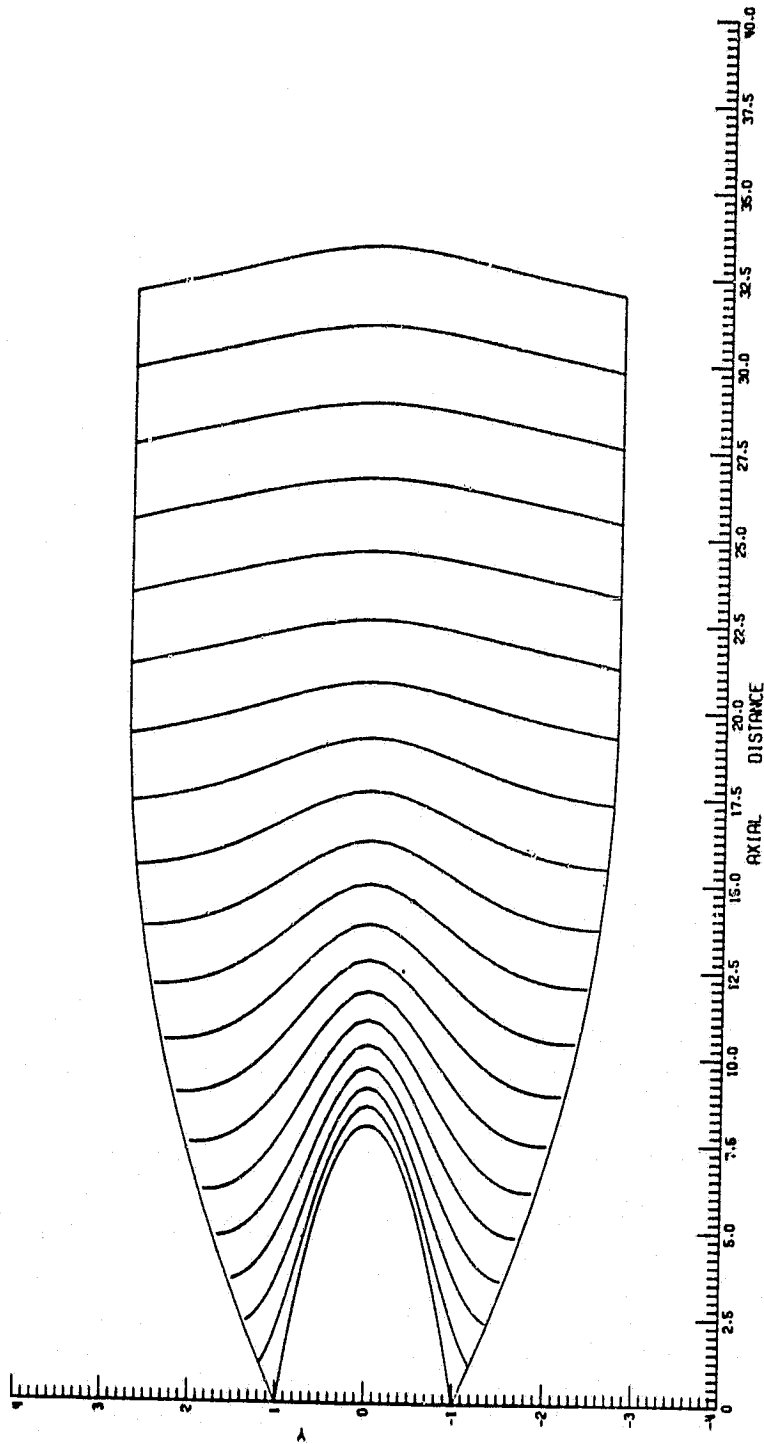


Fig. 8.7a Velocity distribution for a bell-type diffuser, $\alpha = 1$, $\theta = 5$, $L = 20$, $L_t = 32$,
 $Re = 200$.

ORIGINAL PAGE IS
OF POOR QUALITY

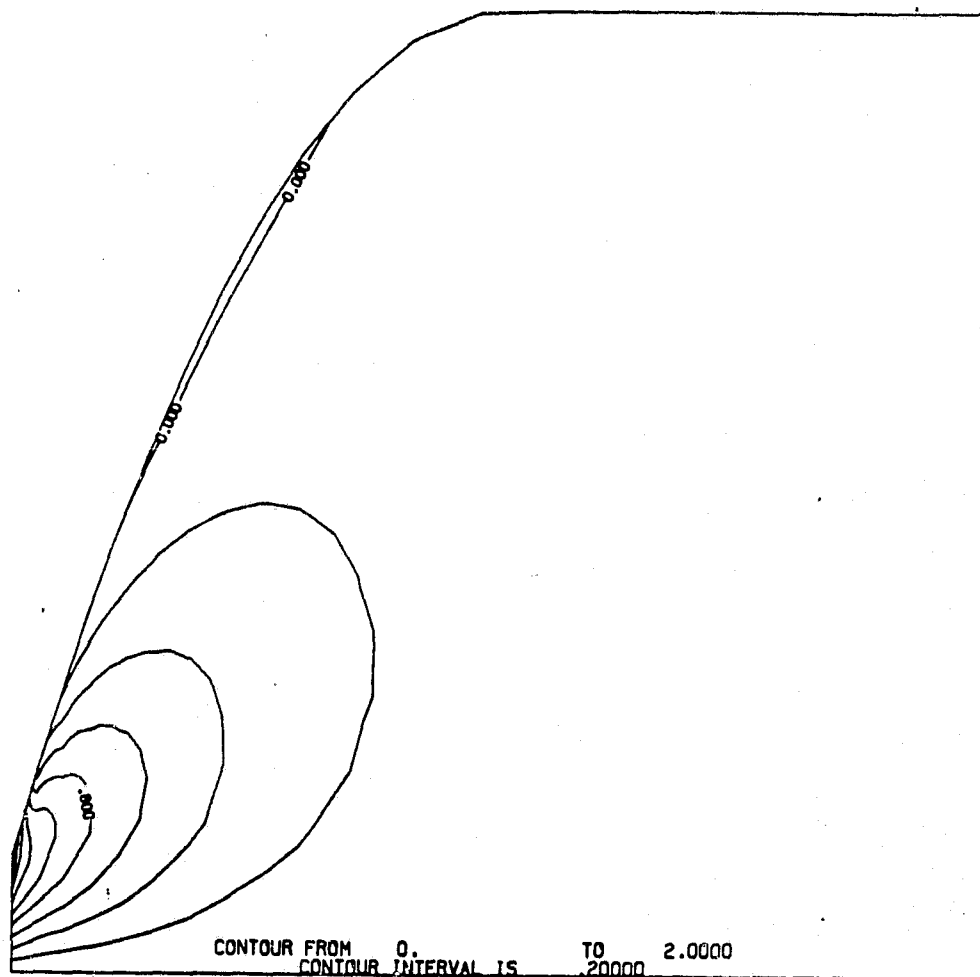


Fig. 8.7b Vorticity contour for a bell-type diffuser,
 $\alpha = 1$, $\theta = 5$, $L = 20$, $L_t = 32$, $Re = 200$.

ORIGINAL PAGE IS
OF POOR QUALITY

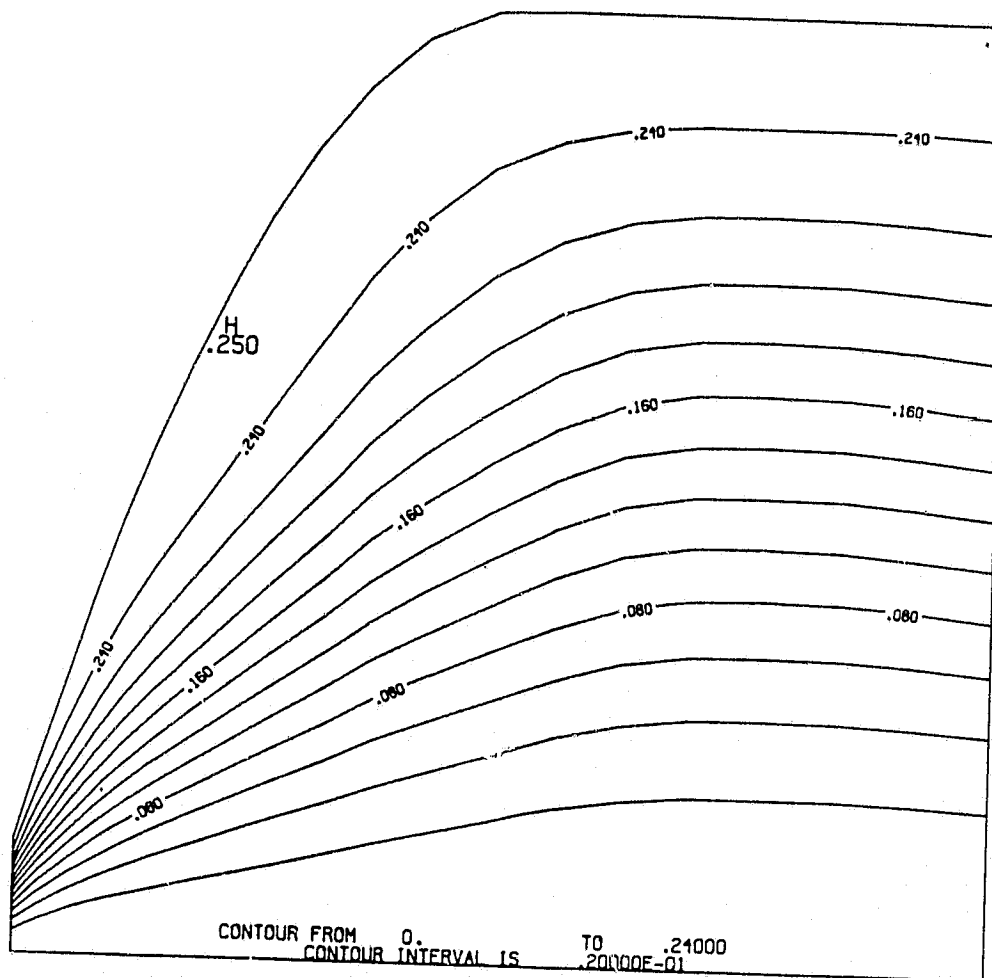


Fig. 8.7c. Stream function contour for a bell-type diffuser,
 $\bar{\alpha} = 1$, $\theta = 5$, $L = 20$, $L_t = 32$, $R_e = 200$.

ORIGINAL PAGE 12
OF POOR QUALITY

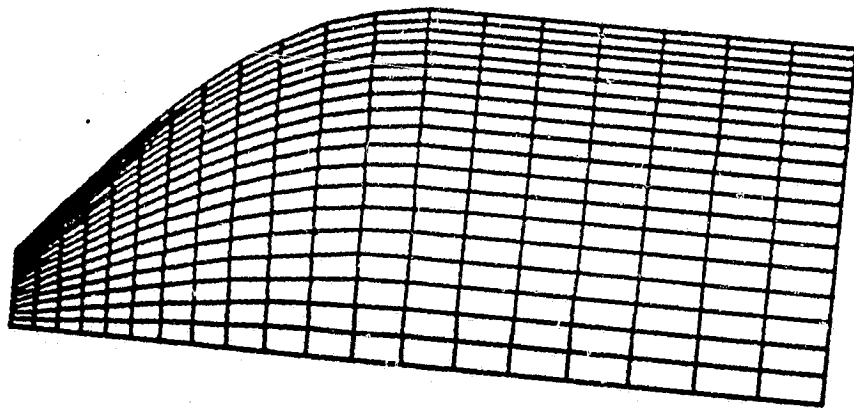


Fig. 8.8 Grid distribution for a bell-type diffuser
 $\bar{\alpha} = 1, \theta = 10, L = 20, L_t = 40.$

ORIGINAL PAGE IS
OF POOR QUALITY

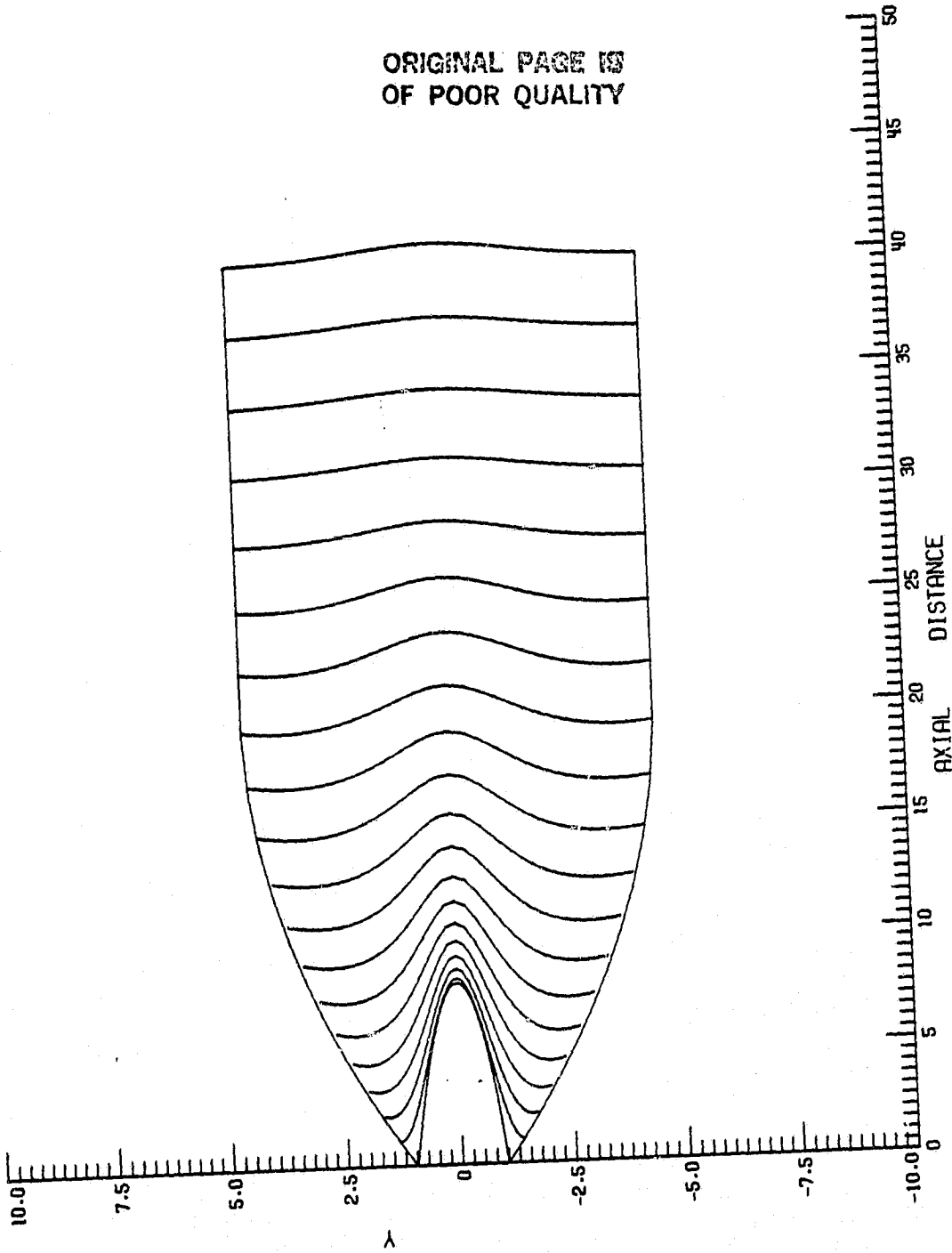


Fig. 8.9a Velocity distribution for a bell-type diffuser, $\bar{\alpha} = 1$, $\theta = 10$, $L = 20$,
 $L_T = 40$, $Re = 200$.

ORIGINAL PAGE IS
OF POOR QUALITY

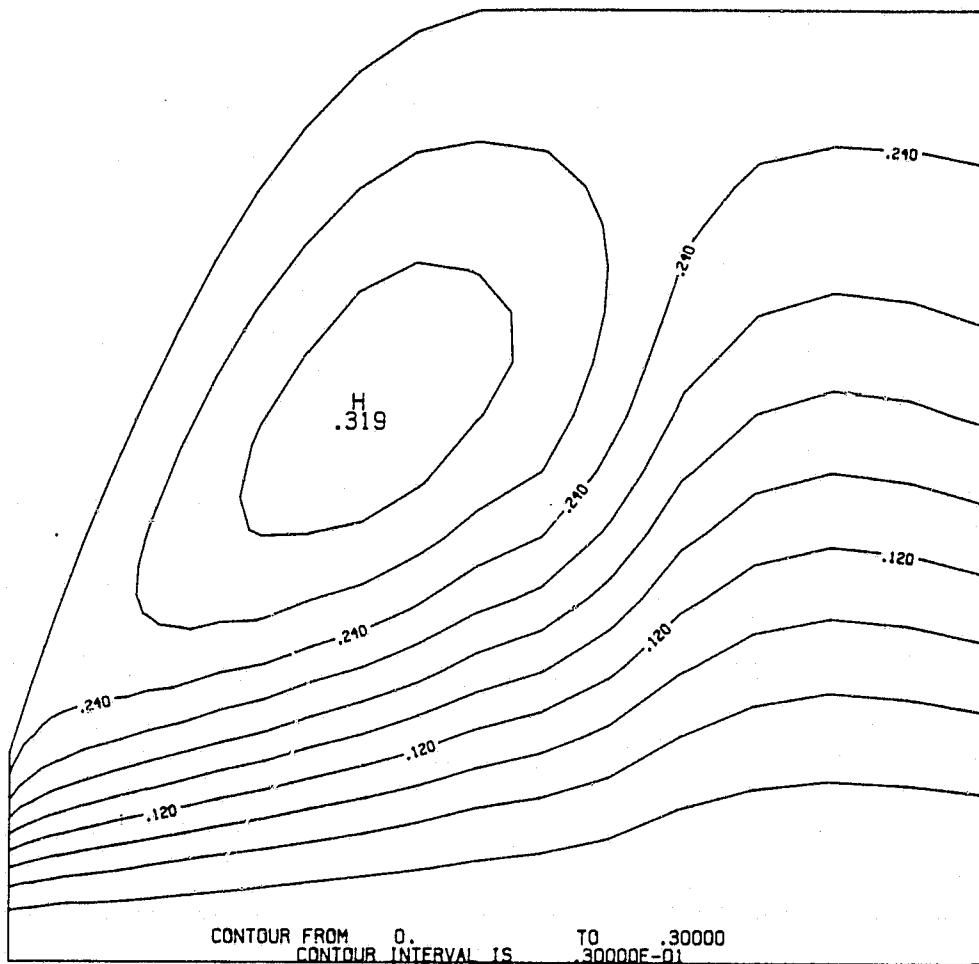


Fig. 8.9b Stream function contour for a bell-type diffuser,
 $\alpha = 1$, $\theta = 10^\circ$, $L = 10^\circ$, $L_t = 40$, $Re = 200$.

ORIGINAL PAGE IS
OF POOR QUALITY

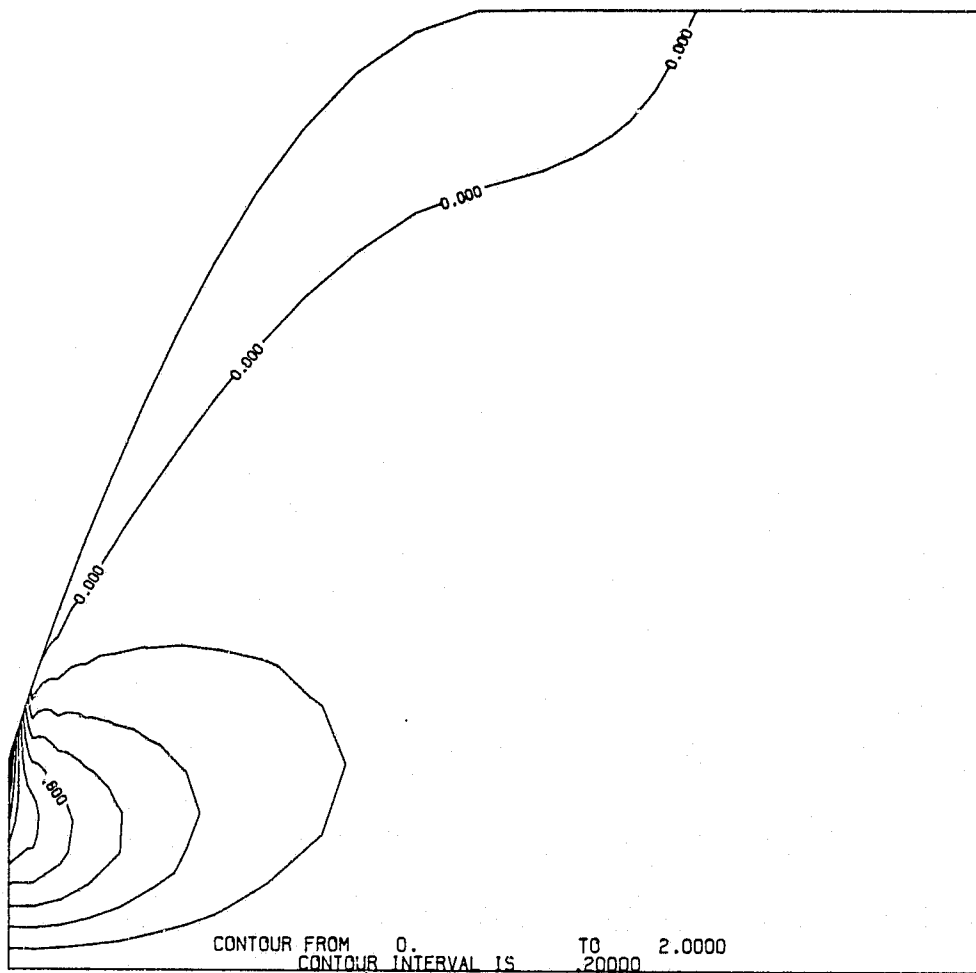


Fig. 8.9c Vorticity contour for a bell-type diffuser, $\bar{\alpha} = 1$,
 $\theta = 5$, $L = 10$, $L_t = 40$, $Re = 200$.

ORIGINAL PAGE 10
OF POOR QUALITY

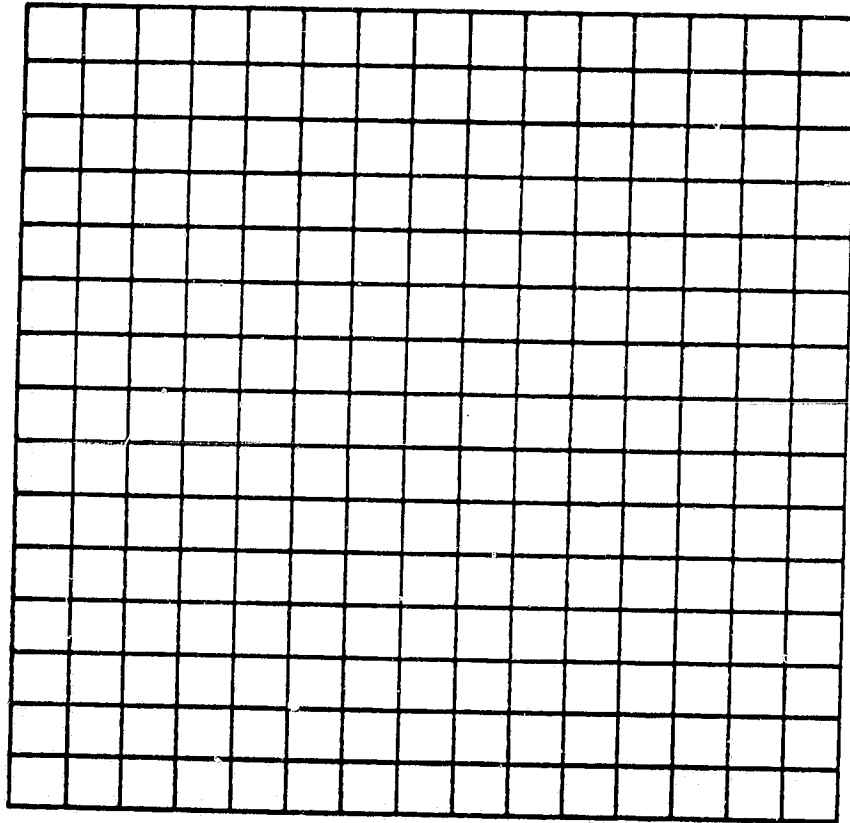
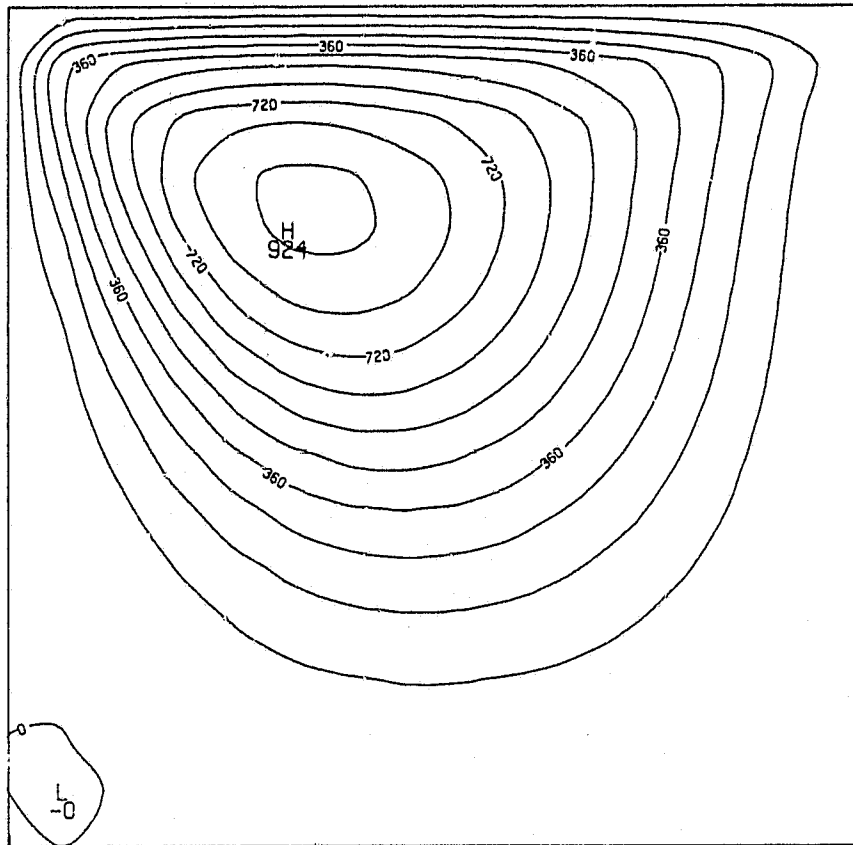


Fig. 8.10 Uniform grid distribution for a driven cavity.

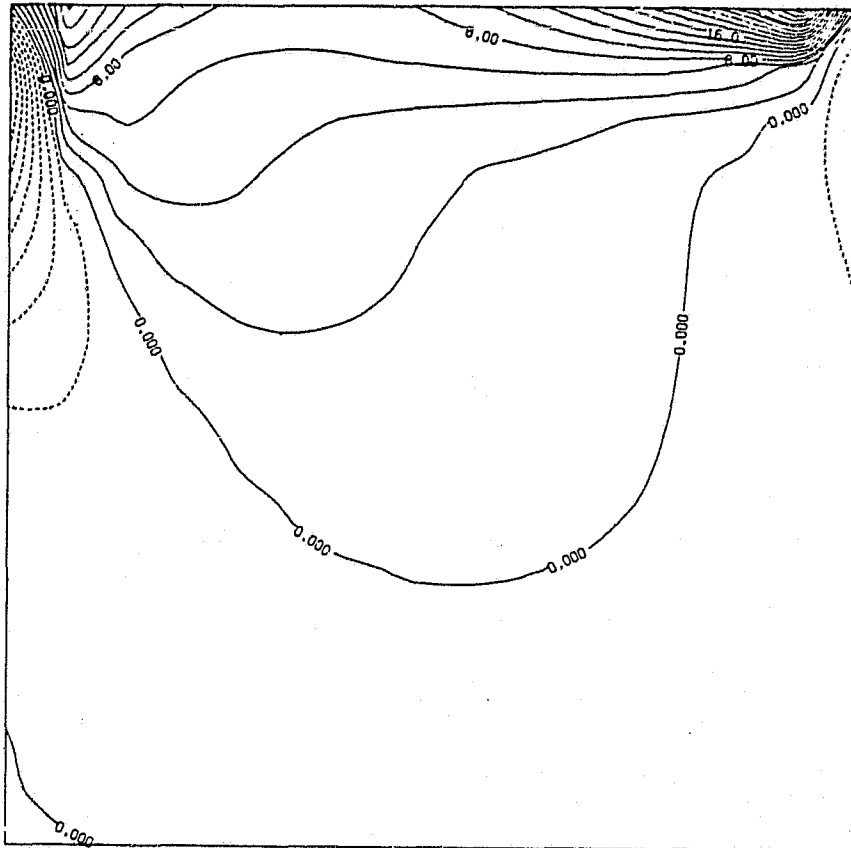
ORIGINAL PAGE IS
OF POOR QUALITY



CONTOUR FROM 0. TC .90000E-01
CONTOUR INTERVAL IS .90000E-02 LABELS SCALED BY 1000.

Fig. 8.11a Stream function distribution for uniform grid distribution, $Re = 100$.

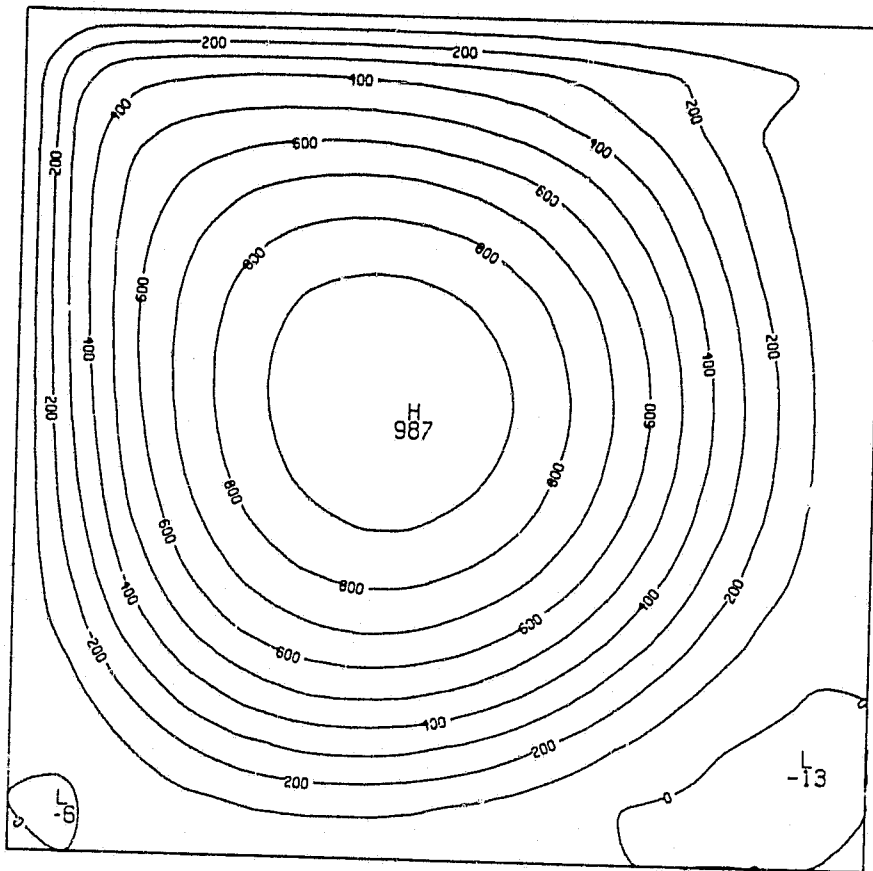
ORIGINAL PAGE IS
OF POOR QUALITY



CONTOUR FROM -14.000 TO 34.000
CONTOUR INTERVAL IS 2.0000

Fig. 8.11b Vorticity distribution for uniform grid
distribution, $Re = 100$.

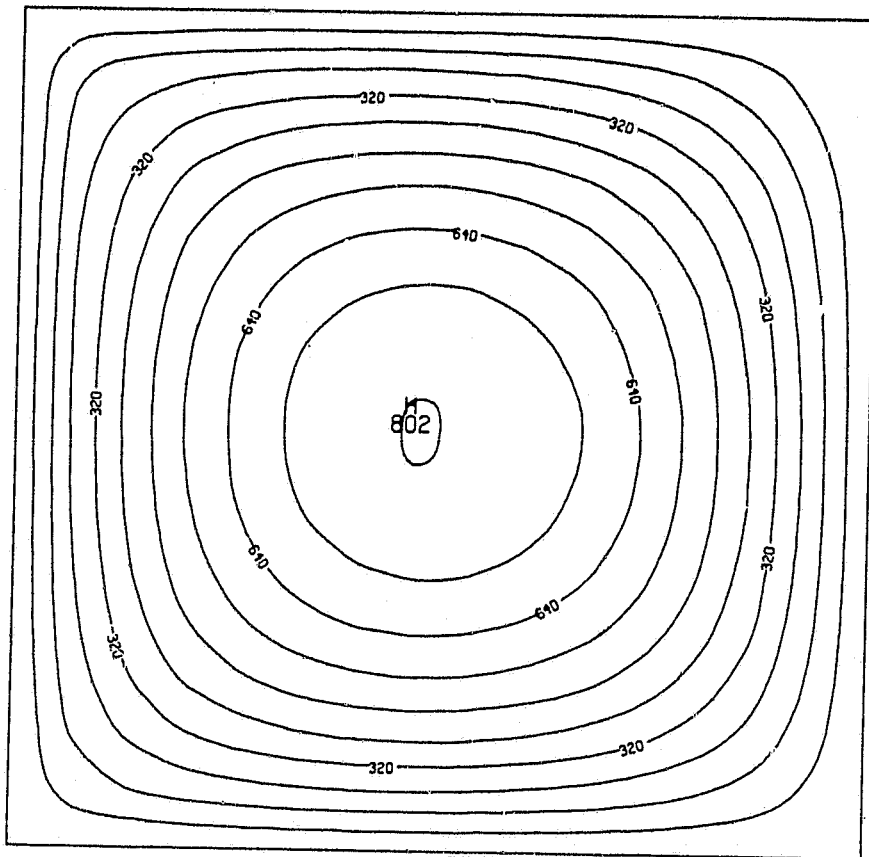
ORIGINAL PAGE IS
OF POOR QUALITY



CONTOUR FROM -16.000 TO 38.000
CONTOUR INTERVAL IS 2.0000

Fig. 8.12a Stream function distribution for uniform grid distribution, $Re = 1,000$.

ORIGINAL PAGE IS
OF POOR QUALITY



CONTOUR FROM 0. TO .80000E-01
CONTOUR INTERVAL IS .80000E-02 LABELS SCALED BY 10000.

Fig. 8.13a Stream function distribution for uniform grid distribution, $Re = 10,000$.

flow consists essentially of a single inviscid core of vorticity with viscous effects being confined to a thin shear layer near the wall boundaries. By using a nonuniform grid distribution, Fig. 8.14, solutions were obtained for Reynolds numbers of 100 and 1000. As shown in Fig. 8.14, the grids are concentrated near the corners in order to capture the secondary vorticities. The results are shown in Figs. 8.15 and 8.16 for $Re=100$ and 1000, respectively. The secondary vorticities are captured, but the results are not in good agreement with those obtained previously. The maximum value of the primary streamlines is 30 percent lower than the results obtained with uniform grid distribution. Accuracy can be gained by using finer grids but this will result in higher computer costs.

ORIGINAL PAGE IS
OF POOR QUALITY

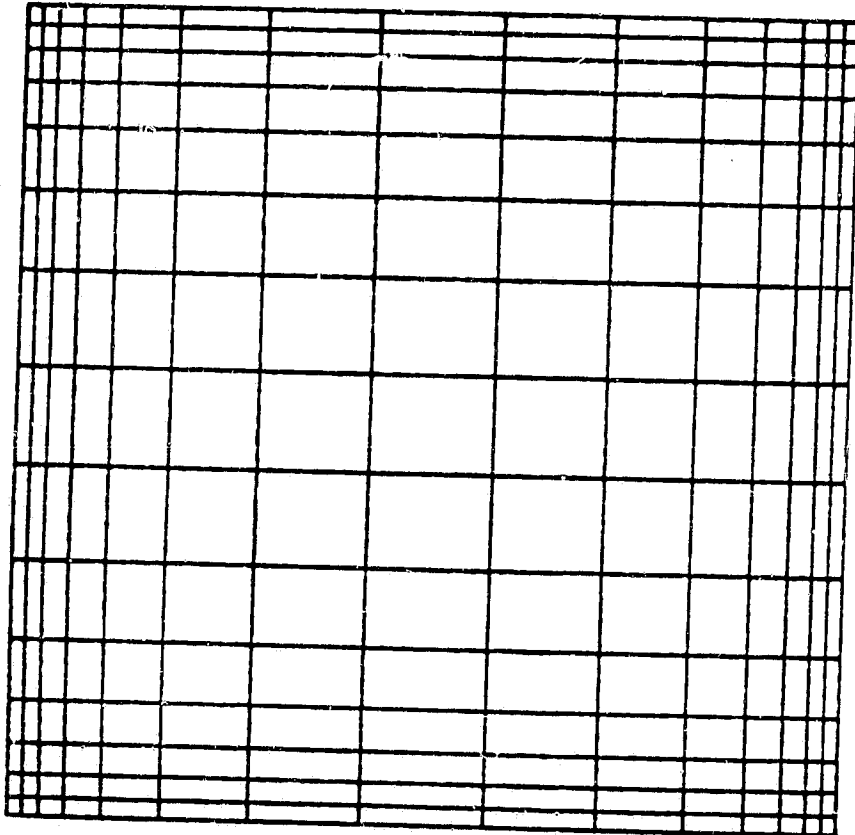
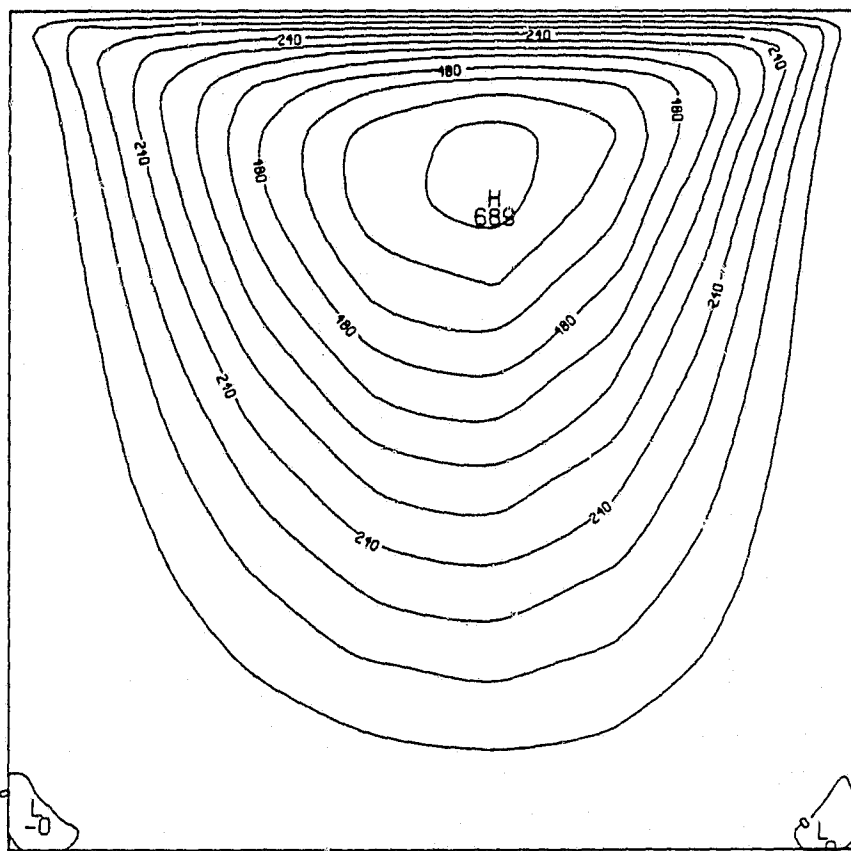


Fig. 8.14 Nonuniform grid distribution for a driven cavity.

C-2.

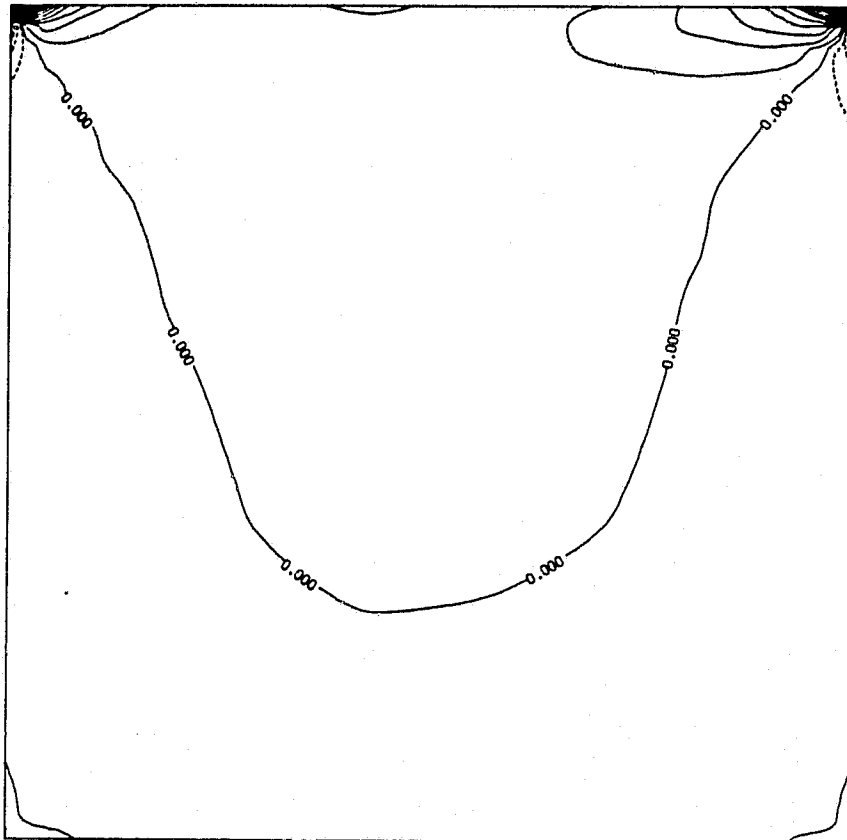
ORIGINAL PAGE IS
OF POOR QUALITY



CONTOUR FROM 0. TO .66000E-01
CONTOUR INTERVAL IS .60000E-02 LABELS SCALED BY 10000.

Fig. 8.15a Stream function distribution for nonuniform grids, $Re = 100$.

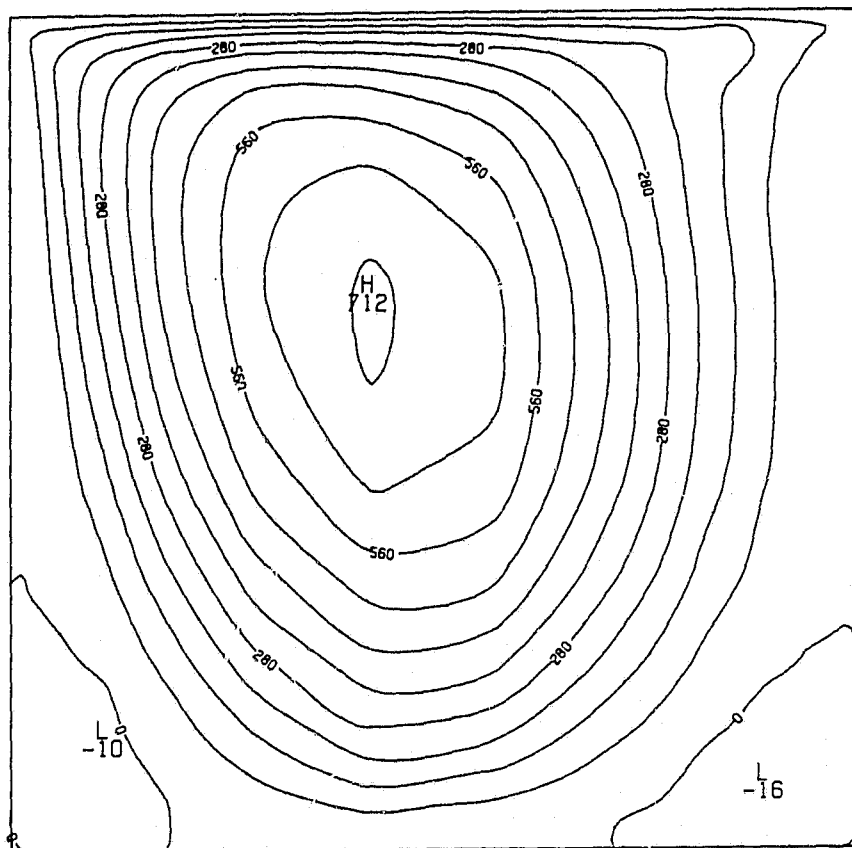
ORIGINAL PAGE IS
OF POOR QUALITY



CONTOUR FROM -12.000 TO 112.00
CONTOUR INTERVAL IS 7.0000

Fig. 8.15b Vorticity distribution for nonuniform grids,
Re = 100.

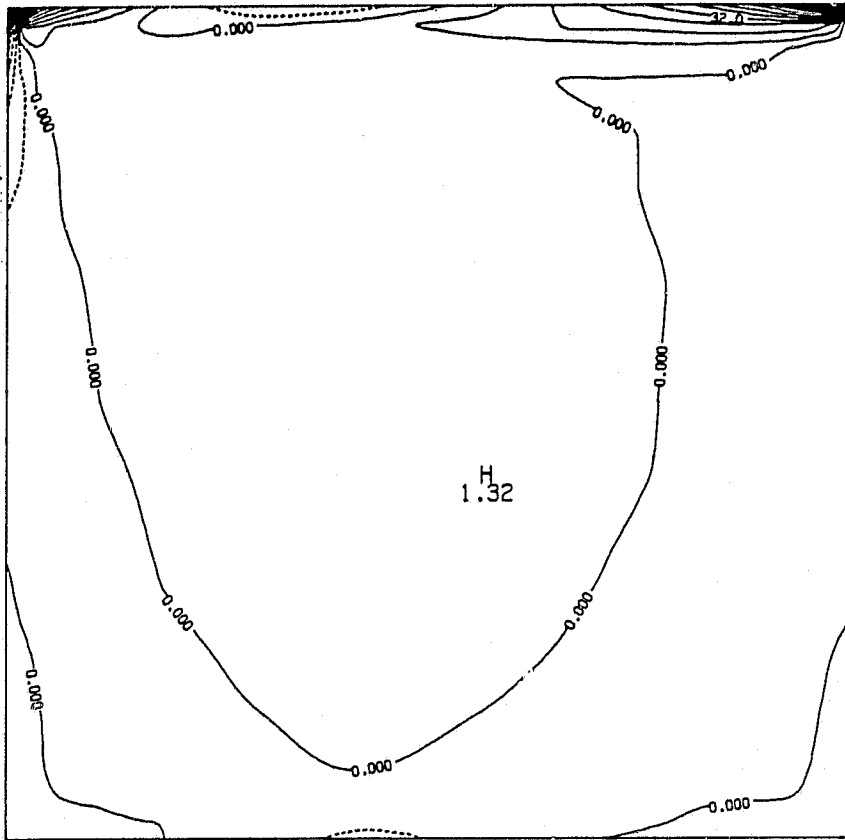
ORIGINAL PAGE IS
OF POOR QUALITY



CONTOUR FROM 0. TO .70000E-01
CONTOUR INTERVAL IS .70000E-02 LABELS SCALED BY 10000.

Fig. 8.16a Stream function distribution for nonuniform grids, $Re = 1,000$.

ORIGINAL PAGE IS
OF POOR QUALITY



CONTOUR FROM -40.000 TO 120.00
CONTOUR INTERVAL IS 8.0000

Fig. 8.16b Vorticity distribution for nonuniform grids,
 $Re = 1,000$.

Chapter 9

CONCLUSIONS

The main objective of this study has been to investigate the feasibility of the method of lines for application to physical problems with nonuniform grid distributions. To attain this objective, it has been necessary to investigate the stiffness characteristics of the pertinent equations.

The following conclusions are drawn from the analysis of stiff differential equations: (1) equations become stiffer as grids are concentrated, (2) the slope of the stiffness characteristic curve is higher near the fixed boundary ($x=0$) than near the derivative boundary ($x=1$), (3) equations become stiffer for a large number of grid points, (4) use of forward differencing is not feasible, (5) the step size is inversely proportional to the Reynolds number for central differencing, and (6) backward differencing is preferable over central differencing at high Reynolds numbers. These conclusions are based on the analysis of one-dimensional heat conduction and fluid flow equations.

The viability and validity of the method of lines are illustrated with applications to the Navier-Stokes equations. A computer program is developed to solve Eqs. (2.21) and (2.22), and the details of this program are available in [38]. This method is quite convenient from a programming point of view, but computational costs are relatively higher compare to the standard finite difference technique. The computational procedure used in this study does not require any local linearization in the governing equations. The method has been applied successfully to obtain solutions for flow in parallel ducts

curved-wall diffusers and a driven cavity. Most solutions have been obtained by using the non-conservative form of the governing equations. The results are in good agreement with other available results for flow in parallel ducts. The solutions also predict the flow development and separation in the curved-wall diffusers. For the case of a driven cavity, the results obtained by using the non-conservative form of equations are valid only up to a Reynolds number of 100. At higher Reynolds numbers the non-conservative equations provide spurious results. The conservative form of the equations was used to obtain results up to Reynolds number of 10,000. Both counter rotating secondary vortices are captured by using a nonuniform grid distribution where grids are concentrated near the walls. However, there is a loss of accuracy in the primary vortex. The results are in good agreement with results of other investigations.

The analysis of flow in a driven cavity indicates that at a Reynolds number of 100, the flow is viscous in the primary vortex with little indication of an inviscid core. The inviscid core region has filled much of the cavity with viscous regions confined near the walls at a Reynolds number of 1000. At a Reynolds number of 10,000, however, the inviscid core has completely filled the cavity with small viscous regions very close to the wall. These results indicate that the flow in a cavity can be characterized by a large vortex adjacent to the moving wall and small counter-rotating vortices in the corners.

The results show the validity and viability of the method of lines where the physical domain is covered with a variable mesh. For further study, it is recommended to include the following: (1) use a

larger number of grid points, (2) solve the stream function equation by a more powerful method, (3) use a higher order approximation for the vorticity equation, and (4) write the available codes for a vector computer such as the CYBER 203 so that finer grids can be used.

REFERENCES

1. Liskovets, O. A., "The Method of Lines (Review)," Differential Equations, Vol. 1, December 1965, pp. 1308-1323.
2. Leser, T. and J. T. Harrison, "The Method of Lines for Numerical Solutions of Partial Differential Equations," Ballistic Research Laboratories Report No. 1311 (N66-3842), March 1966.
3. Hicks, J. S. and J. Wei, "Numerical Solution of Parabolic Partial Differential Equations with Two-Point Boundary Conditions by Use of the Method of Lines," Journal of the Association for Computing Machinery, Vol. 14, No. 3, July 1967, pp. 549-562.
4. Klunker, E. B., J. C. South and R. M. Davis, "Calculation of Non-linear Conical Flows by the Method of Lines," NASA-TRR-374, October 1971.
5. Jones, D. J., J. C. South and E. B. Klunker, "On the Numerical Solution of Elliptic Partial Differential Equations by the Method of Lines," Journal of Computational Physics, Vol. 9, June 1972, pp. 496-527.
6. Madsen, N. K. and R. E. Sincovec, "The Numerical Method of Lines for the Solution of Nonlinear Partial Differential Equations," Lawrence Livermore Laboratory (Technical Report N78-74702), September 1973.
7. Hamilton, II, H. H., "Solution of Axisymmetric and Two-Dimensional Inviscid Flow Over Blunt Bodies by the Method of Lines," NASA-TP-1154 (N78-22332), April 1978.
8. Kurtz, L. A., R. E. Smith, C. L. Parks and L. R. Boney, "A Comparison of the Method of Lines to Finite Difference Techniques in Solving Time-Dependent Partial Differential Equations," Computer and Fluids, Vol. 6, August 1979, pp. 49-70.
9. Annon., Computer Science Corporation CSC, "Subroutine Voadam, Vol. II, Section D2.2," NASA Langley Research Center, Hampton, Virginia, November 1973.
10. Loeb, A. M. and W. E. Schiesser, "Stiffness and Accuracy in the Method of Lines Integration of Partial Differential Equations, Part I and Part II, "Proceeding of the 1973 Summer Computer Simulation Conference (Sponsored by AICHE/AMS/ISA/SCS/SHARE), Montreal, Canada, 1973, pp. 25-39.

11. Smith, R. E. and A. Kidd, "Comparative Study of Two Numerical Techniques for the Solution of Viscous Flow in a Driven Cavity," Numerical Studies of Incompressible Viscous Flow in a Driven Cavity, NASA SP-378, 1975.
12. Roache, P. J., Computational Fluid Dynamics, Hermosa Publisher, 1972.
13. Morris, D. J., "Solution of the Incompressible Driven Cavity Problem by the Alternative-Direction Implicit Method," Numerical Studies of Incompressible Viscous Flow in a Driven Cavity, NASA SP-378, 1975.
14. Gear, C. W., Numerical Initial Value Problems in Ordinary Differential Equations, Prentice-Hall, Englewood Cliffs, New Jersey, 1971.
15. Lapidus, L. and J. H. Seinfeld, Numerical Solution of Ordinary Differential Equations, Academic Press, New York, 1971.
16. Shampine, L. F. and M. K. Gordon, Computer Solution of Ordinary Differential Equations: Initial Value Problem, W. H. Freeman and Company, San Francisco, 1975.
17. Hindmarsh, A. C., Gear Ordinary Differential Equation System Solver, Lawrence Livermore Laboratory, University of California, Rep. UCID-30001, Rev. 3, December 1974.
18. Annon., Computer Science Corporation CSC, "Subroutine REGR, Vol. II, Section F 2.3," NASA Langley Research Center, Hampton, Virginia, November 1973.
19. Paris, J. and S. Whitaker, "Confined Wakes: A Numerical Solution of the Navier-Stokes Equations," American Institute of Chemical Engineers Journal, Vol. 11, No. 6, November 1965, pp. 1033-1041.
20. Thoman, D. and A. A. Szewczyk "Time Dependent Viscous Flow Over A Circular Cylinder," The Physics of Fluids Supplement II, Vol. 12, December 1969, pp. 76-87.
21. Briley, W. R., "A Numerical Study of Laminar Separation Bubbles Using the Navier-Stokes Equations," Journal of Fluid Mechanics, Vol. 47, Part 4, June 1971, pp. 713-736.
22. Roache, P. J. "Sufficiency Conditions for a Commonly Used Downstream Boundary Condition on Stream Function," Journal of Computational Physics, Vol. 6, October 1970, pp. 317-321.
23. Ghia, U., K. N. Ghia, S. G. Rubin and P. K. Khosla, "Study of Incompressible Flow Separation Using Primitive Variable," Computer and Fluids, Vol. 9, June 1981, pp. 123-142.

24. Moretti, G., "Grid Generation Using Classical Techniques," Proceedings of Numerical Grid Generation Techniques (Sponsored by NASA Langley), NASA Conference Publication 2166, Hampton, Virginia, October 1980.
25. Thompson, J. F. and C. W. Mastin, "Grid Generation Using Differential Systems Techniques," Proceedings of Numerical Grid Generation Techniques (Sponsored by NASA Langley), NASA Conference Publication 2166, Hampton, Virginia, October 1980.
26. Smith, R. E. and B. L. Weigel, "Analytical and Approximate Boundary Fitted Coordinate Systems for Fluid Flow Simulation," Aerospace Sciences Meeting (Sponsored by American Institute of Aeronautics and Astronautics), Pasadena, California, January 14-16, 1980.
27. Thompson, J. F., Z. U. A. Warsi and C. W. Mastin, "Review Article: Boundary Fitted Coordinate Systems for Numerical Solution of Partial Differential Equations," Journal of Computational Physics, Vol. 47, July 1982, pp. 1-108.
28. Schlichting, H., Boundary Layer Theory, Seventh Edition, McGraw-Hill Book Co., New York, 1979.
29. Campbell, W. D. and J. C. Slattery, "Flow in Entrance of a Tube," Journal of Basic Engineering, Vol. 85, March 1963, pp. 41-46.
30. Sparrow, E. M., S. H. Shin and T. S. Lundgren, "Flow Development in the Hydrodynamic Entrance Region of Tubes and Ducts," The Physics of Fluids, Vol. 7, No. 3, March 1964, pp. 338-347.
31. Van Dyke, M., "Entry Flow in a Channel," Journal of Fluid Mechanics, Vol. 44, Part 4, December 1970, pp. 813-823.
32. Vrentas, J. S., J. L. Duda and K. G. Barger, "Effect of Axial Diffusion of Vorticity on Flow Development in Circular Conduits," American Institute of Chemical Engineering Journal, Vol. 12, No. 5, September 1966, pp. 837-844.
33. Atkinson, G. S. and S. Goldstein, Modern Developments in Fluid Dynamics, Vol. 1, Oxford, 1934.
34. Kawaguti, M., "Numerical Solution of the Navier-Stokes Equation for the Flow in a Two-Dimensional Cavity," Journal of Physical Society of Japan, Vol. 16, No. 12, November 1961, pp. 2307-2315.
35. Burggraf, O. R., "Analytical and Numerical Studies of the Structure of Steady Separated Flow," Journal of Fluid Mechanics, Vol. 24, Part 1, January 1966, pp. 113-151.

36. Bozeman, J. D. and C. Dalton, "Numerical Study of Viscous Flow in a Driven Cavity," Journal of Computational Physics, Vol. 12, July 1973, pp. 348-363.
37. Schreiber, R. and H. B. Keller, "Driven Cavity Flows by Efficient Numerical Techniques," Journal of Computational Physics, Vol. 49, February 1983, pp. 310-333.
38. Abolhassani, J. S., "Application of the Method of Lines for Solutions of the Navier-Stokes Equations Using A Nonuniform Grid Distribution," Masters Thesis, School of Engineering, Old Dominion University, Norfolk, Virginia 23508, May 1983.